Dose computation

Methods and algorithms

Jean Michel LÉTANG

CREATIS

CENTRE DE LUTTE CONTRE LE CANCER LEON BERARD

INSA INSTITUT NATIONAL DES SCIENCES APPLIQUÉES LYON

Tuesday, July 9

Preamble

- Focus on dose for external radiotherapy mainly
- Review of standard dose algorithms
- No exam at the end!
- Feel free to interrupt for any question or remark

Plan

Terminology

Fluence: The number of photons of energy E passing through a unit cross-sectional area is referred to as the fluence Φ and is typically expressed in units of cm^{-2}.

$$\Phi(E) = \frac{\mathrm{Photons\,(E)}}{\mathrm{Area}}$$

Fluence rate: The rate at which photons of energy E pass through a unit area ($\perp$ to the propagation) per unit time is called the flux.

$$\dot{\Phi}(E) = \frac{\mathrm{Photons\,(E)}}{\mathrm{Area} \times \mathrm{Time}}$$

Energy fluence: The amount of energy passing through a unit cross-sectional area is referred to as the energy fluence

$$\Psi(E) = \Phi(E) \times E$$

Interaction components

(Ahnesjö and Aspradakis 1999)

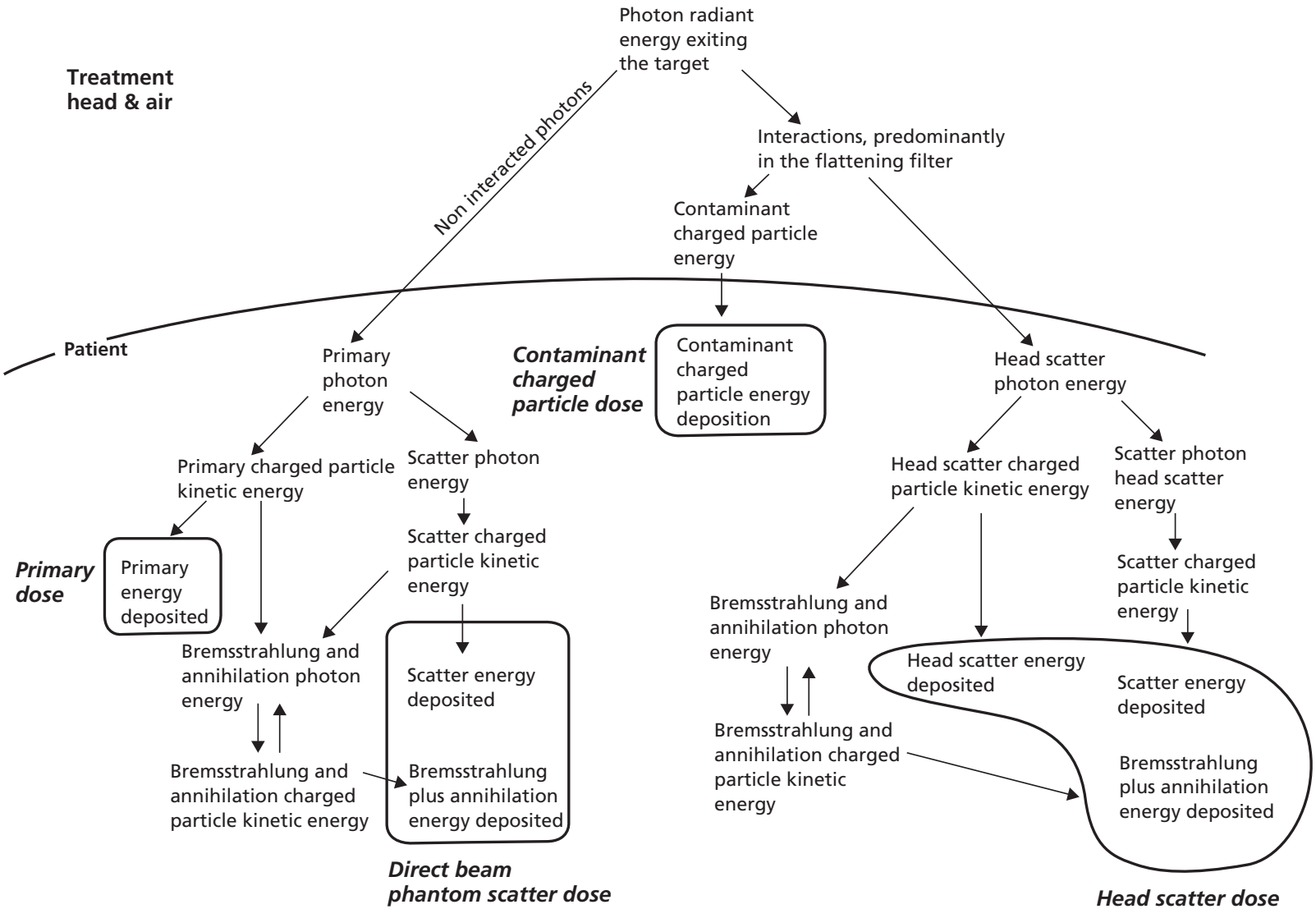

Linear attenuation coefficient μ

Beer-Lambert attenuation law

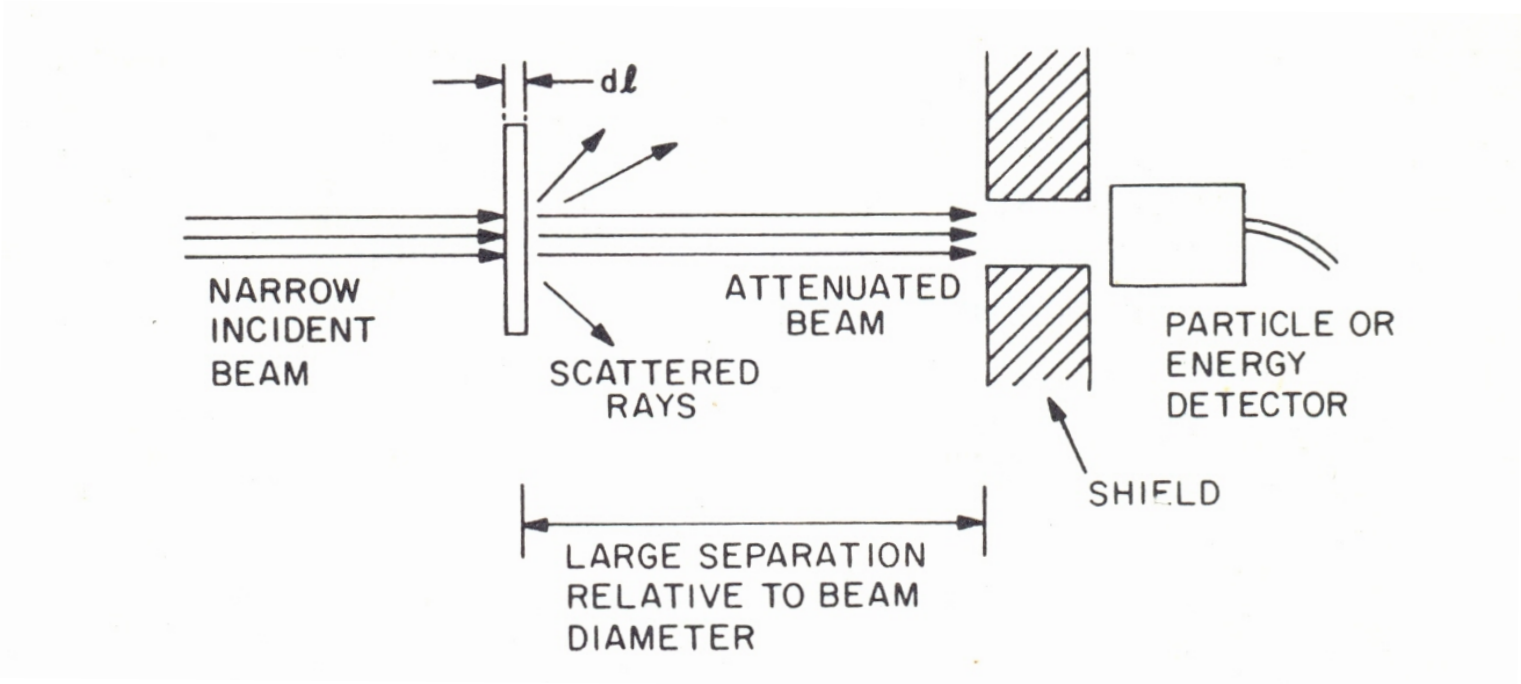

$$dN = -\mu\, N\, dl$$

or μ can be defined as a percentage of interaction per unit length as

$$\mu = \frac{|dN|\,/N}{dl}$$

Photon propagation

Beer-Lambert attenuation law

$$N_{\mathrm{DT}}(E) = N_0(E)\ \exp\left(-\int_{\mathbf{r}\in\mathrm{ray}} \mu(\mathbf{r}, E)\,\mathrm{d}\mathbf{r}\right)$$

Divergence

$$\Psi(r, E) \propto \frac{1}{r^2}$$

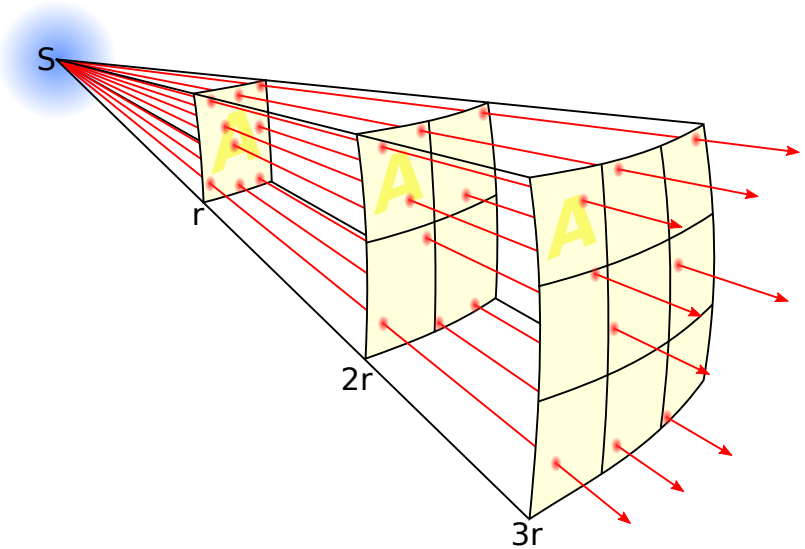

Mean Free-Path (MFP)

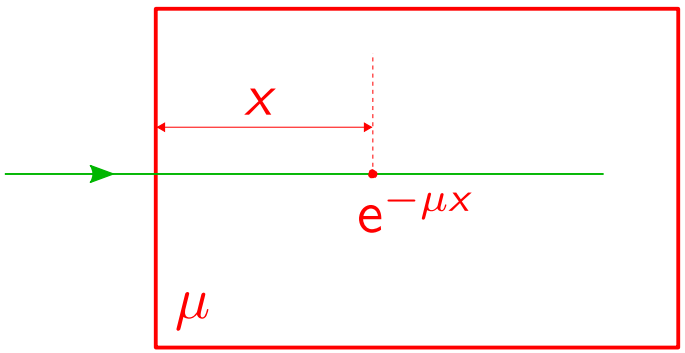

Mean Free Path (in cm): **average distance** x_1 to the **first interaction**

$$T_{\text{MFP}} = \langle x_1 \rangle = \int_0^\infty \mu x \, e^{-\mu x} \, \mathrm{d}x = \left[-x e^{-\mu x} \right]_0^\infty + \int_0^\infty e^{-\mu x} \, \mathrm{d}x = 0 + \left[\frac{-1}{\mu} e^{-\mu x} \right]_0^\infty$$

MFP

$$T_{\text{MFP}} = \frac{1}{\mu}$$

Dose

Dose is the absorbed energy per unit mass:

$$D = \frac{E_{\text{absorbed}}}{m} \quad \text{expressed in Gy (gray) or J kg}^{-1}.$$

NB: to boil 1 g of water $\Rightarrow$ 100 calories $\equiv$ 418 J/g $=$ 418 kGy! (only in MRT)

Dose

$$D(\mathbf{r}, E) = \Psi(\mathbf{r}, E) \times \mu_{\text{en}}(\mathbf{r}, E)/\rho(\mathbf{r})$$

where $\mu_{\text{en}}(\mathbf{r}, E)$ is the linear **energy-absorption** coefficient at $\mathbf{r}$

$\Rightarrow$ relation with the linear attenuation coefficient $\mu(E)$?

Total energy released per unit mass

Given

- $\Psi(\mathbf{r}, E)$ is the total energy fluence,
- $\mu(\mathbf{r}, E)$ is the percentage of interaction per unit length

Energy transfered to all secondary particles per unit mass is:

TERMA

$$T(\mathbf{r}, E) = \Psi(\mathbf{r}, E) \times \mu(\mathbf{r}, E)/\rho(\mathbf{r})$$

NB:

- TERMA is also the divergence of the energy fluence $\Psi(\mathbf{r}, E)$
- Only a fraction of the incident photon energy is transfered to electrons $\Rightarrow \mu_{\text{tr}}$ & KERMA

Linear energy-transfer coefficient μ_{tr}

$$\mu_{\text{tr}}(E) = \sum_{k \in \{\text{RS,CS,PE,PP}\}} f_k(E)\ \mu_k(E)$$

where fractions $f_k(E)$ can defined by subtracting the radiative 2^{ary} parts:

$$f_{\text{RS}}(E) = 1 - 1 = 0$$

$$f_{\text{CS}}(E) = 1 - \langle E_{\text{sc}} \rangle / E$$

$$f_{\text{PE}}(E) = 1 - \langle X \rangle / E$$

$$f_{\text{PP}}(E) = 1 - 2 m_e c^2 / E$$

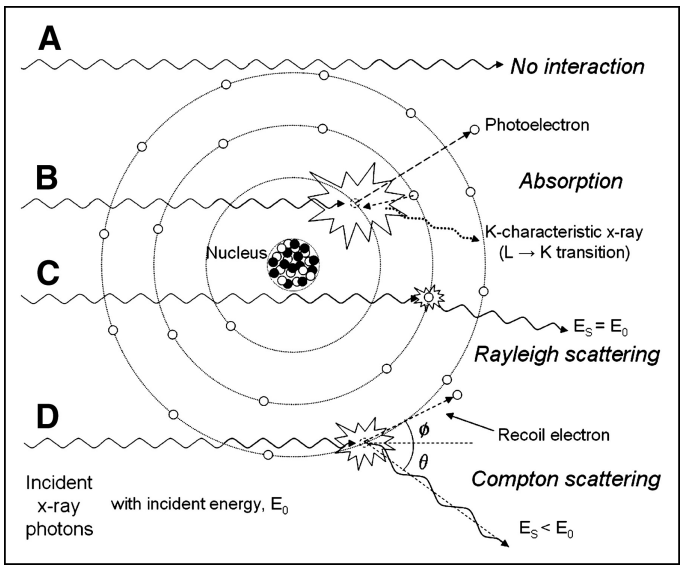

given

- $\langle X \rangle$ the average fluorescence energy,
- $\langle E_{\text{sc}} \rangle$ the average scattered energy.

$\Rightarrow$ Kinetic energy released (to electrons) per unit mass

KERMA

$$K(\mathbf{r}, E) = \Psi(\mathbf{r}, E) \times \mu_{\text{tr}}(\mathbf{r}, E)/\rho(\mathbf{r}) \ < \ T(\mathbf{r}, E)$$

Linear energy-absorption coefficient μ_{en}

Electrons may experience radiative losses: **Fluorescence** & **Bremsstrahlung**

Linear energy-absorption coefficient μ_{en}:

$$\mu_{\text{en}}(E) = (1 - g(E))\ \mu_{\text{tr}}(E)$$

where g is the average fraction of the kinetic energy that is subsequently lost in radiative energy-loss processes.

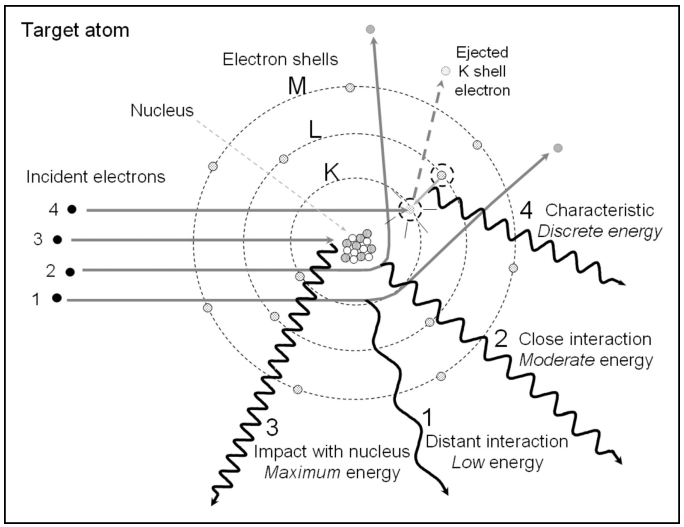

Dose

$$D(\mathbf{r}, E) = \Psi(\mathbf{r}, E) \times \frac{\mu_{\text{en}}(\mathbf{r}, E)}{\rho(\mathbf{r})} = \Phi^{e^-}(\mathbf{r}, E) \frac{S_c(\mathbf{r}, E)}{\rho(\mathbf{r})} < K(\mathbf{r}, E)$$

where $S_c(\mathbf{r}, E)$ is the collisional stopping power

Linear energy-absorption μ_{en} vs attenuation μ coefficients

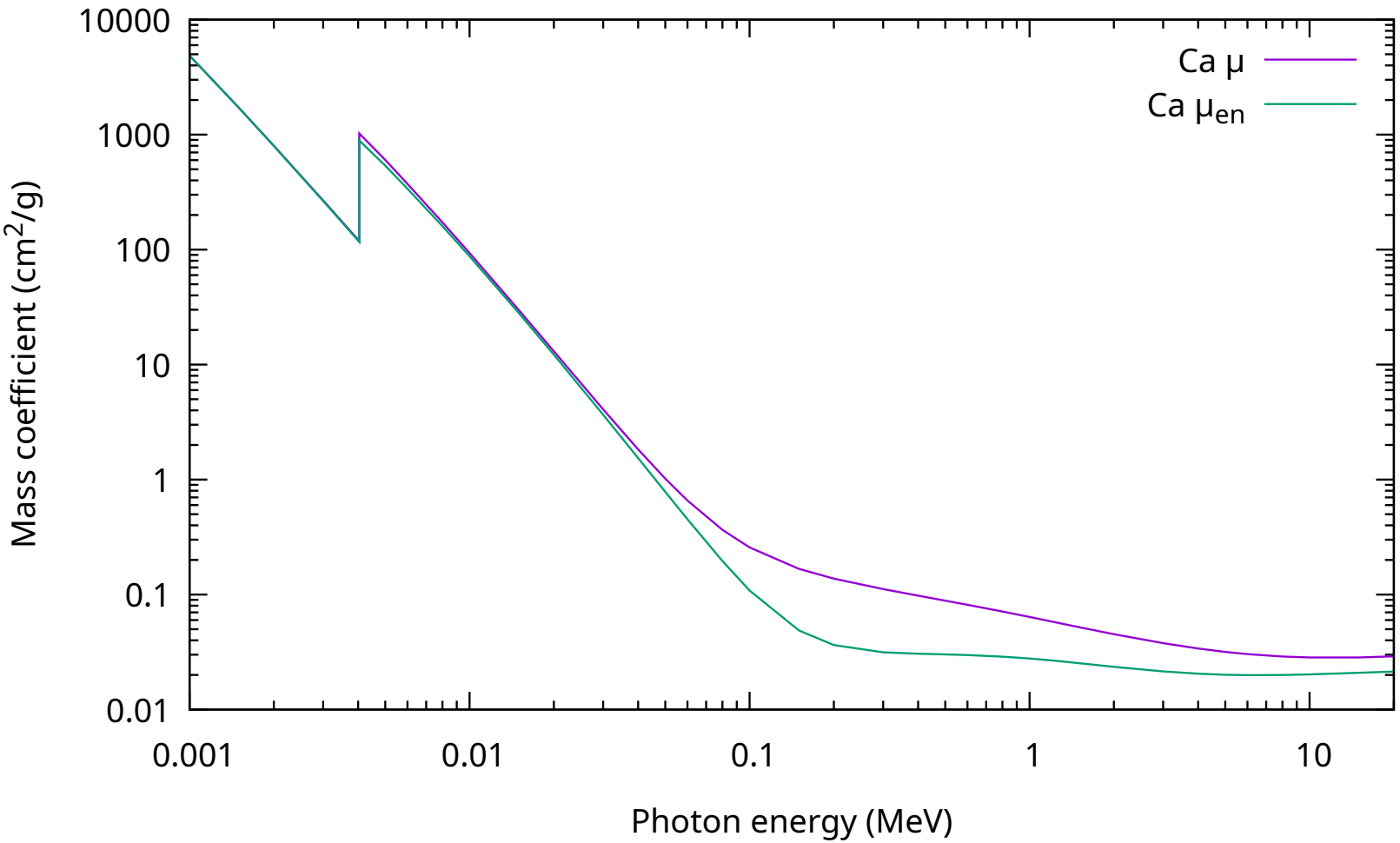

Energy spectrum (LinAc)

(González et al. 2015)

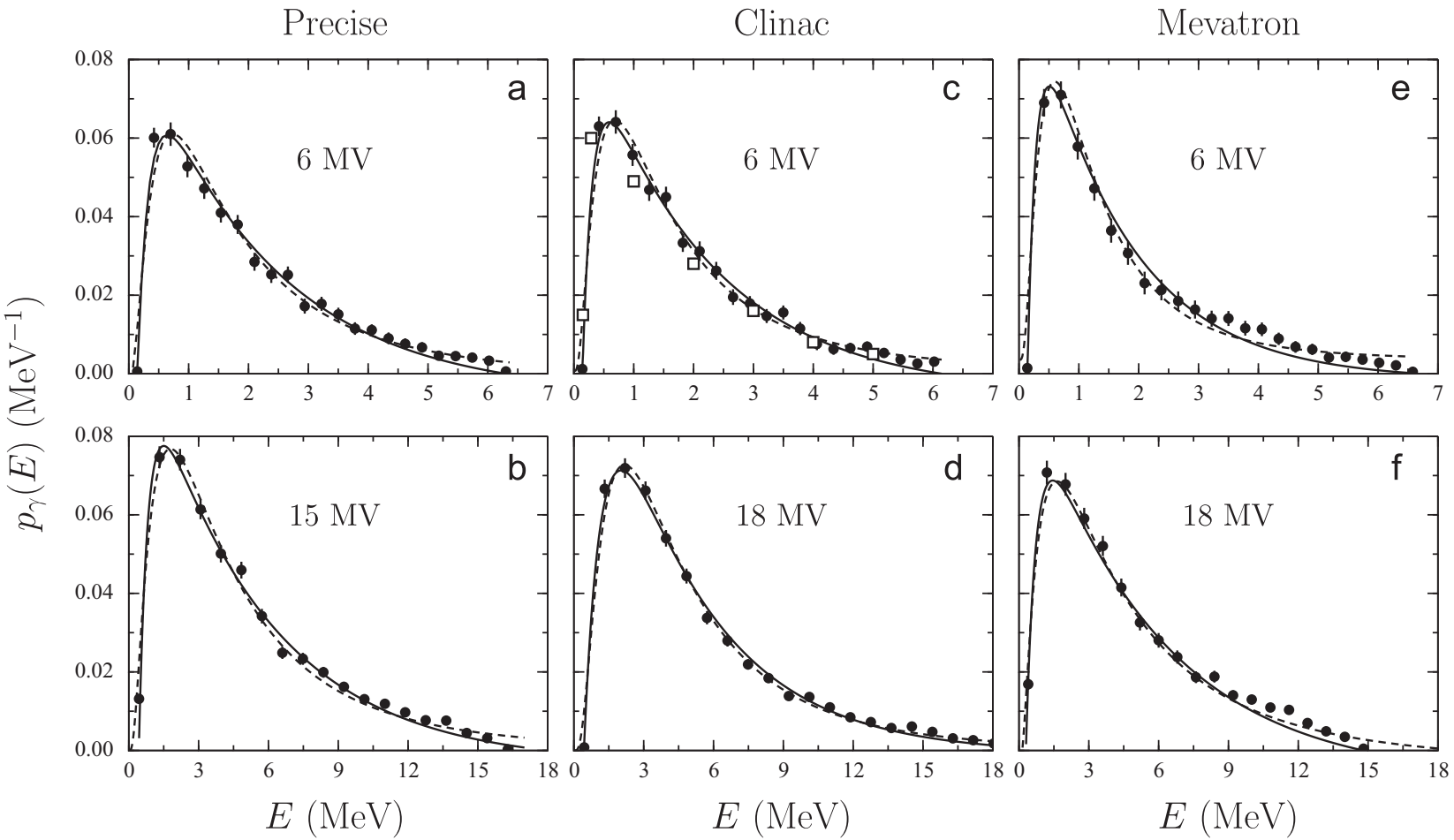

$\Rightarrow$ mean energy 1-3 MeV

Stopping power

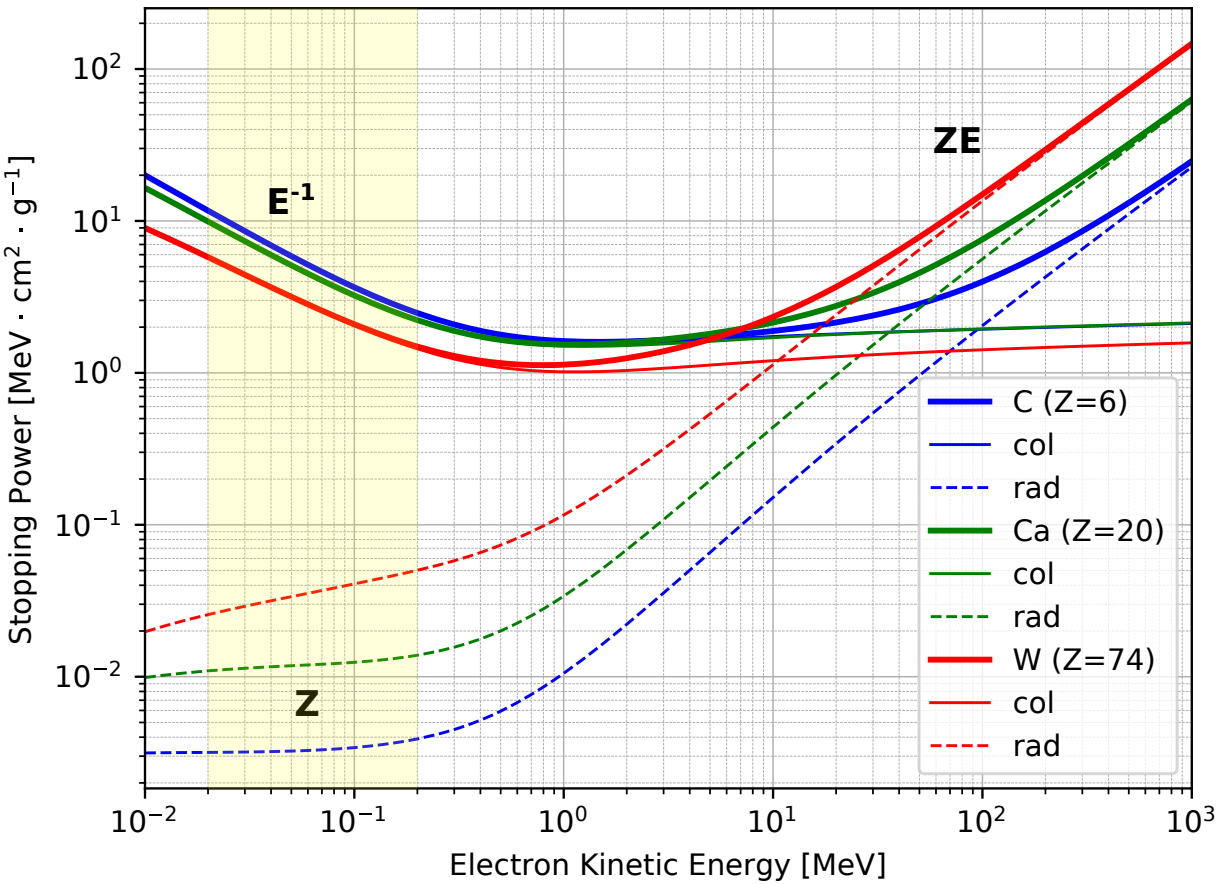

$\Rightarrow$ radiative losses $\ll$ collision losses

CSDA range

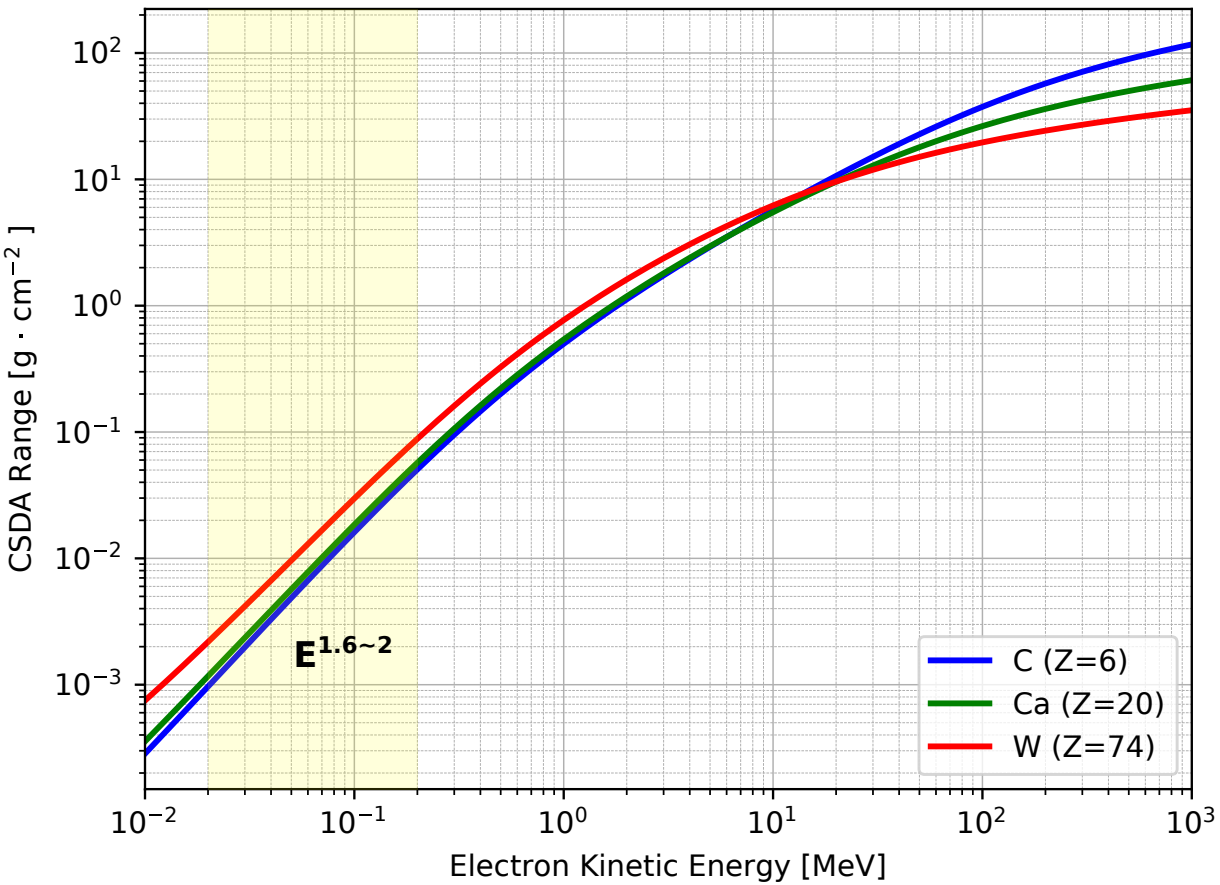

$\Rightarrow$ electrons delocalize the dose

Mass attenuation coefficient μ/ρ ($cm^2 \cdot g^{-1}$) of Carbon

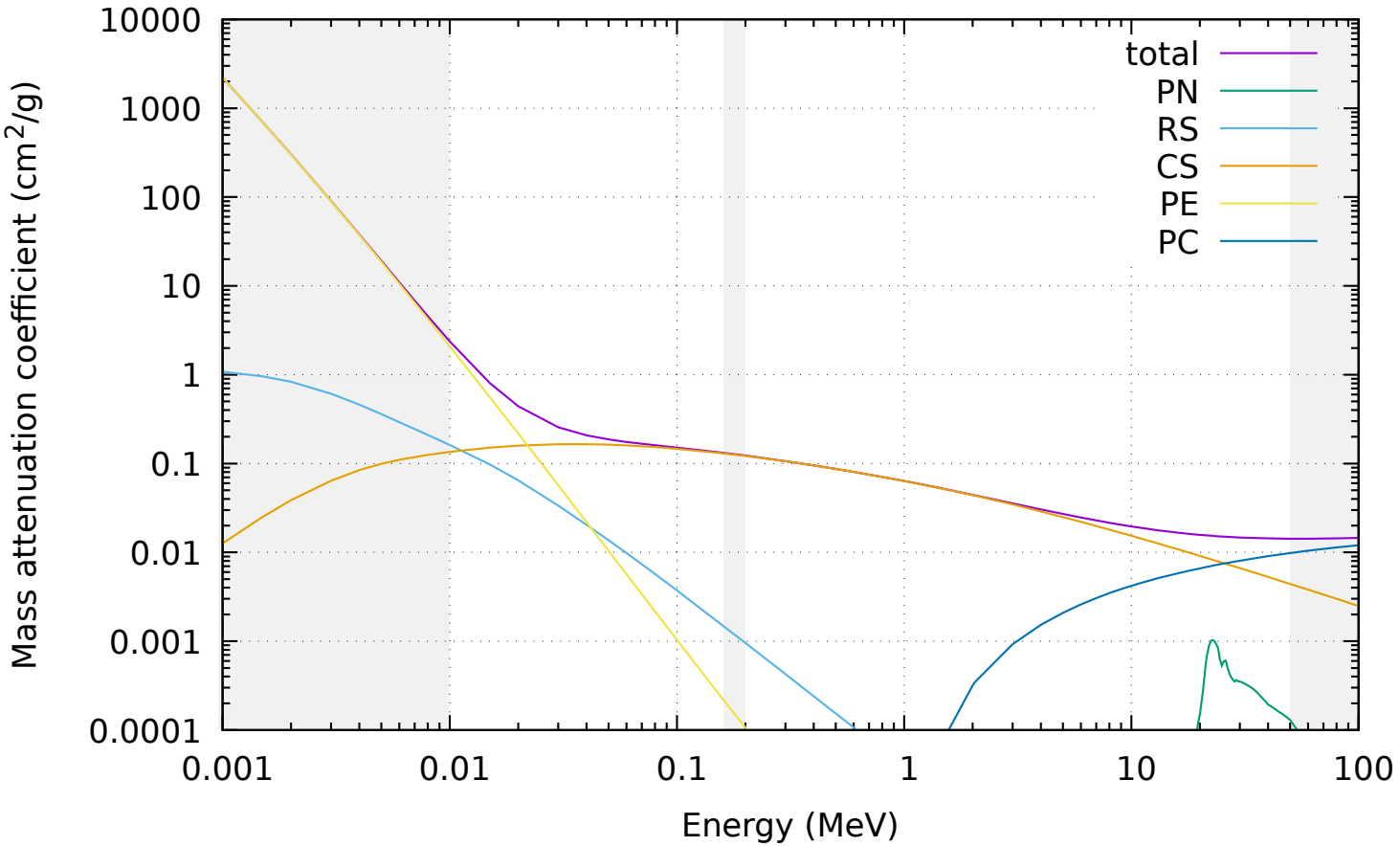

$\Rightarrow$ material scaling only affected by density ratio (not in kV imaging dose)

XCOM `https://www.nist.gov/pml/xcom-photon-cross-sections-database`

JANIS `https://www.oecd-nea.org/janisweb/`

Mass attenuation coefficient μ/ρ ($cm^2 \cdot g^{-1}$) of Calcium

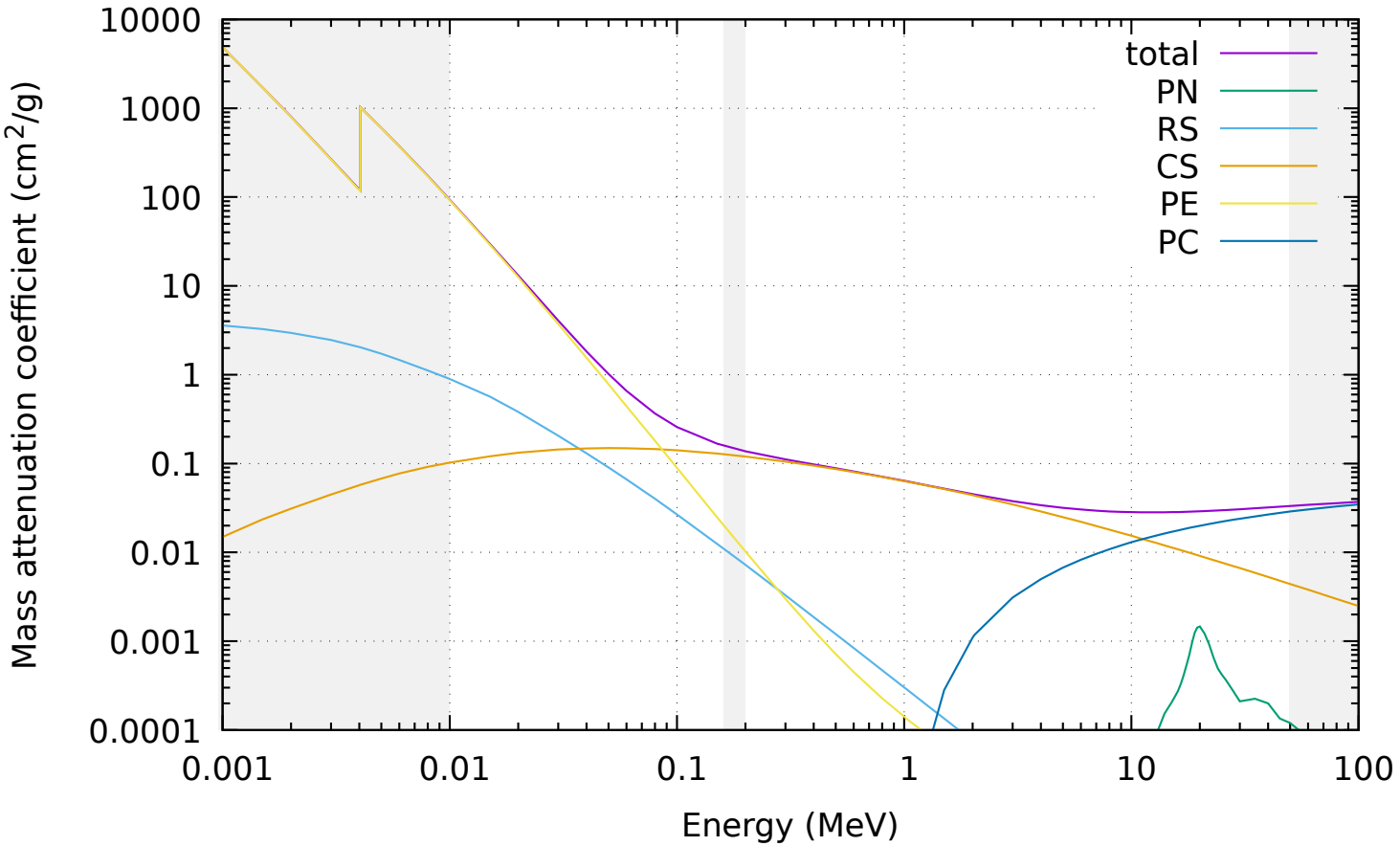

$\Rightarrow$ material scaling only affected by density ratio (not in kV imaging dose)

XCOM `https://www.nist.gov/pml/xcom-photon-cross-sections-database`

JANIS `https://www.oecd-nea.org/janisweb/`

Mass attenuation coefficient μ/ρ ($cm^2 \cdot g^{-1}$) of Tungsten

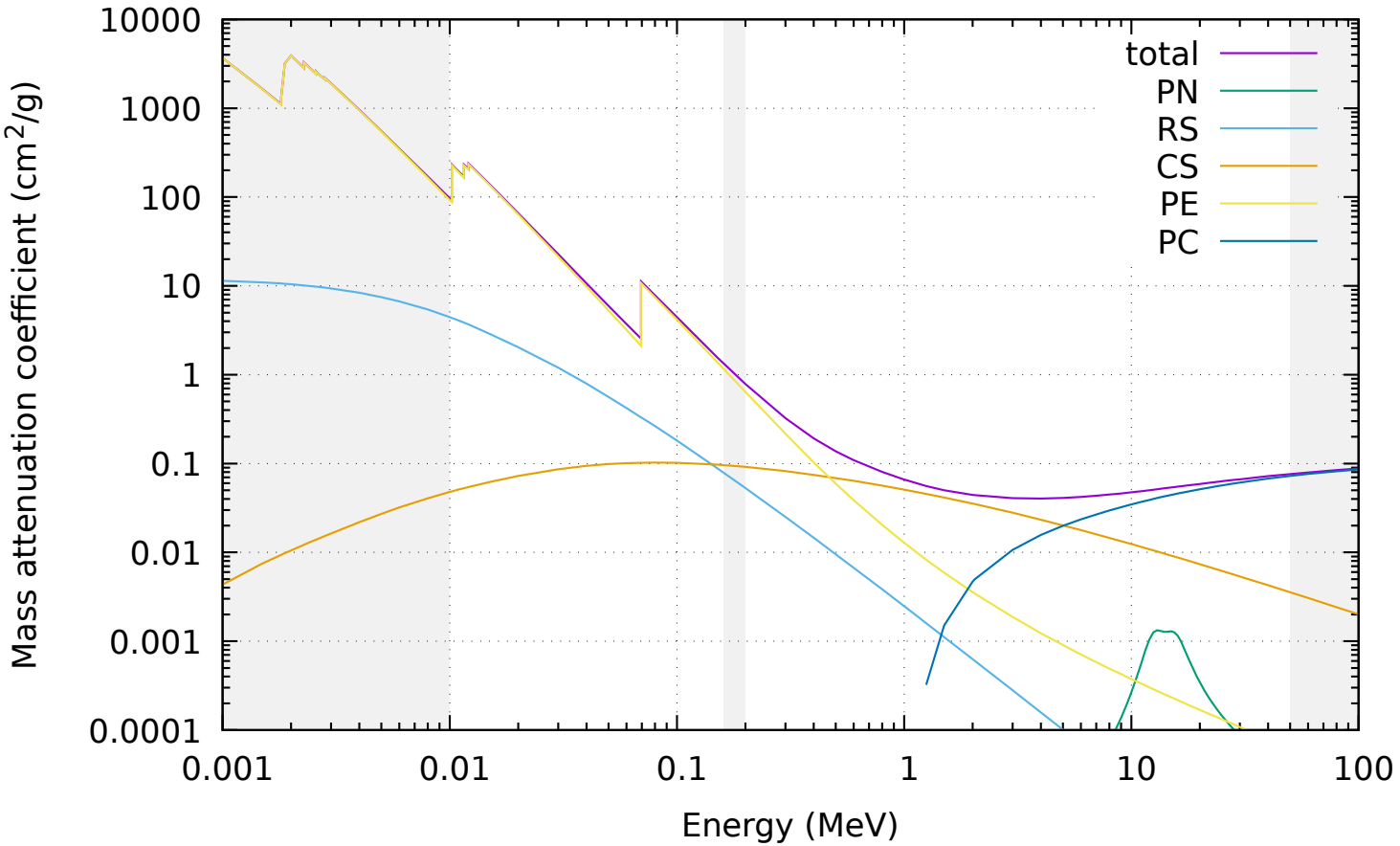

$\Rightarrow$ material scaling only affected by density ratio (not in kV imaging dose)

XCOM `https://www.nist.gov/pml/xcom-photon-cross-sections-database`

JANIS `https://www.oecd-nea.org/janisweb/`

Dose calculation engines

(De Martino et al. 2021)

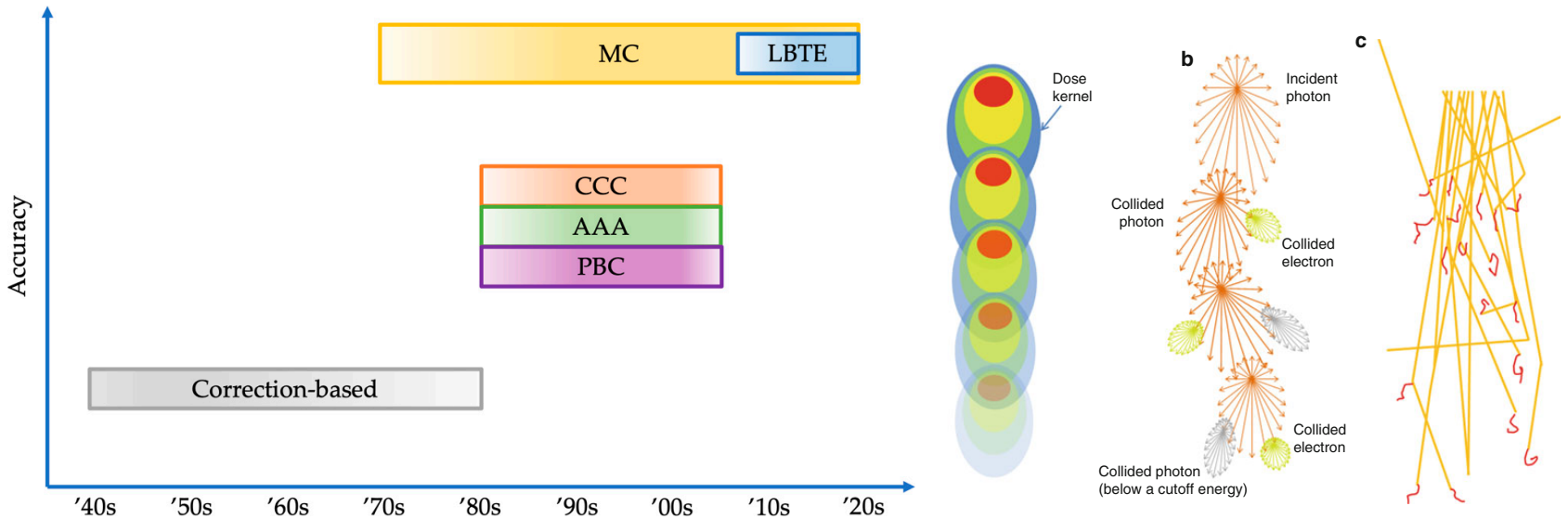

- Early algorithms: Dose measurements in water phantom + corrections (beam penetration, build-up, ...)
- Model-based (eg CT) techniques:
  Convolution, Monte Carlo, Transport Equation

Plan

Point Kernels

(Battista 2019)

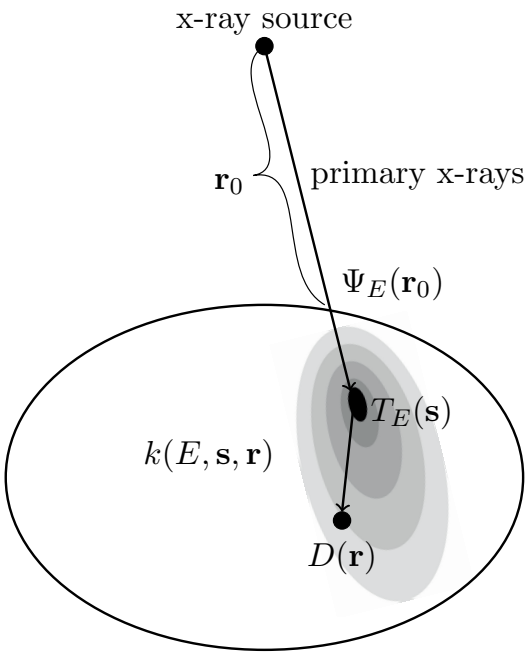

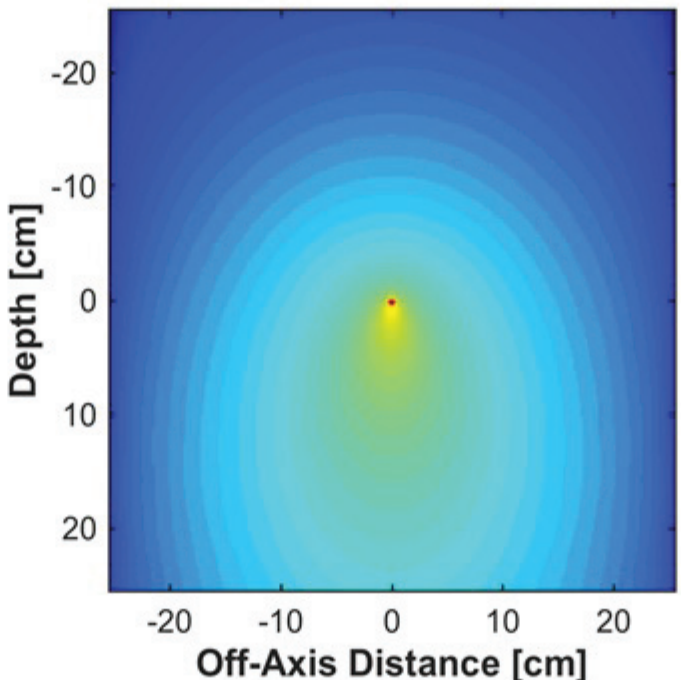

1. compute the TERMA T_E at point s
2. convolve with the kernel to compute dose D at r

Kernel-based method

(convolution/superposition)

Basic ideas:

- Kernels represent the dose deposition of secondary particles stemming from a point irradiation
- Kernels are not (easily) accessible through measurements
  $\Rightarrow$ Monte Carlo calculations.
- Spatial invariance: no edge/border considerations
  $\Rightarrow$ Simulations in large water boxes
- Kernels are normalized to 1 and represented with spherical coordinates

$$\iiint_{\infty} h_E(\mathbf{r})\,\mathrm{d}V \triangleq 1$$

and usually separated into 2 parts: $h_E = h_{\mathrm{prim},E} + h_{\mathrm{scat},E}$ sum of primary dose (e^-) and phantom scatter dose (γ)

$$\iiint_{\infty} h_{\mathrm{prim},E}(\mathbf{r})\,\mathrm{d}V = \frac{\mu_{\mathrm{en},E}}{\mu_E} \quad \text{and} \quad \iiint_{\infty} h_{\mathrm{scat},E}(\mathbf{r})\,\mathrm{d}V = \frac{\mu_E - \mu_{\mathrm{en},E}}{\mu_E}$$

$\Rightarrow$ Kernel model: exponential attenuation and divergence

From Dose to Energy Fluence

Analytical kernels: Homogeneous model

Kernel in water (from Ahnesjö 1989)
= energy released by the 1^{ary} + 2^{ary} photons

$$h(r,\theta) = \frac{A_\theta e^{-a_\theta r}}{r^2} + \frac{B_\theta e^{-b_\theta r}}{r^2}$$

Since the energy deposited per unit volume is the divergence of the vectorial energy fluence

$$h(r,\theta)\ T(s)\ \rho(s)\ \mathrm{d}V = -\nabla \cdot \Psi(r,\theta)$$

and

$$\nabla \cdot \Psi(r,\theta) = \frac{1}{r^2}\frac{\partial}{\partial r}\left(r^2 \Psi(r,\theta)\right)$$

the total energy fluence is

$$\Psi(r,\theta) = T(s)\ \rho(s)\ \mathrm{d}V\ \frac{1}{r^2}\left(\frac{A_\theta}{a_\theta} e^{-a_\theta r} + \frac{B_\theta}{b_\theta} e^{-b_\theta r}\right)$$

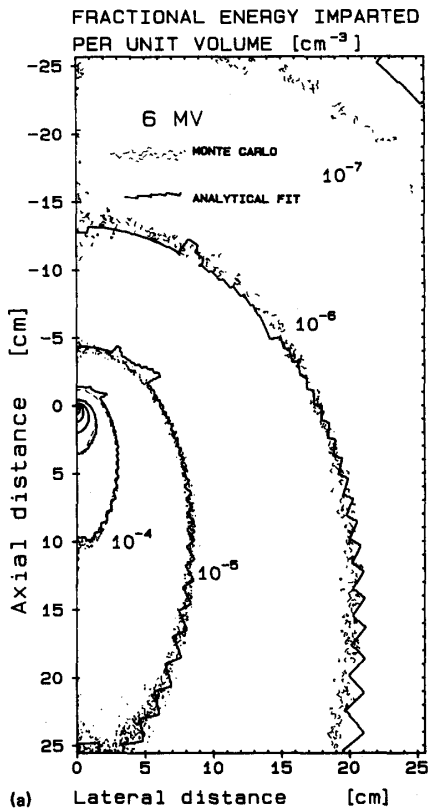

From Energy Fluence to Dose

Analytical kernels: Heterogeneous model

The total energy fluence should be scaled by the relative electron density

$$\Psi(r,\theta) = T(s)\,\rho(s)\,\mathrm{d}V\,\frac{1}{r^2}\left(\frac{A_\theta}{a_\theta}e^{-a_\theta L(r,\theta,\phi)} + \frac{B_\theta}{b_\theta}e^{-b_\theta L(r,\theta,\phi)}\right)$$

where the rectilinear scaling

$$L(r,\theta,\phi) = \int_0^r \eta(t,\theta,\phi)\,\mathrm{d}t \;\approx\; \eta(r,\theta,\phi)\;r$$

and the relative (to water) linear attenuation coefficient

$$\eta(r,\theta,\phi) = \frac{\rho_{e^-}(r,\theta,\phi)}{\rho_{e^-,\mathrm{water}}} \simeq \frac{\mu(r,\theta,\phi)}{\mu_{\mathrm{water}}}$$

We get the analytical expression of the kernel with inhomogeneities

$$h(r,\theta,\phi) = \eta(r,\theta,\phi)\frac{A_\theta e^{-a_\theta L(r,\theta,\phi)} + B_\theta e^{-b_\theta L(r,\theta,\phi)}}{r^2}$$

Balance between kernel components

Primary dose (e^-) vs phantom scatter dose (γ)

- At low energies (< 1 MeV): the electron range is very much shorter than the photon mean free path. A considerable portion of the primary photon energy is also further transported to yield scatter dose.
- At high energies (> 10 MeV) the electron range is of the same order as the photon mean free path. Only a minor part of the primary photon energy is transferred to scatter dose.

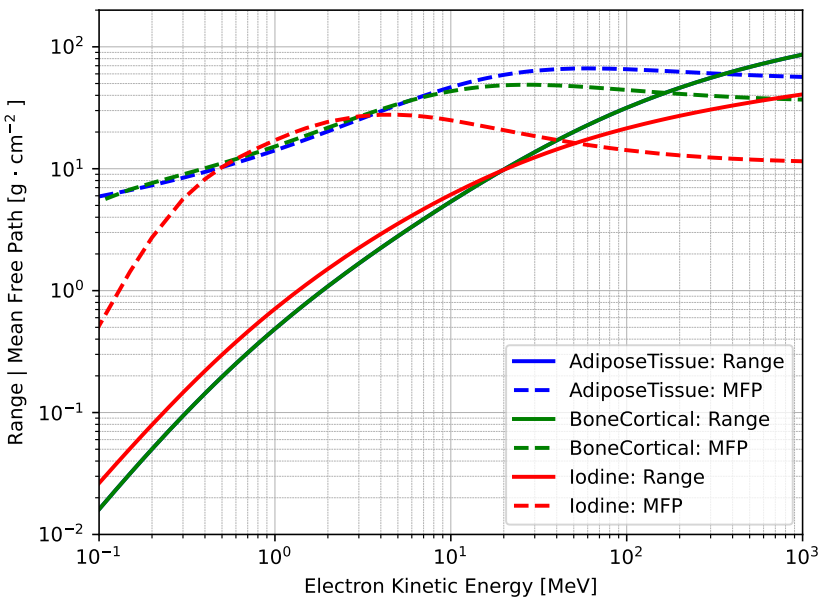

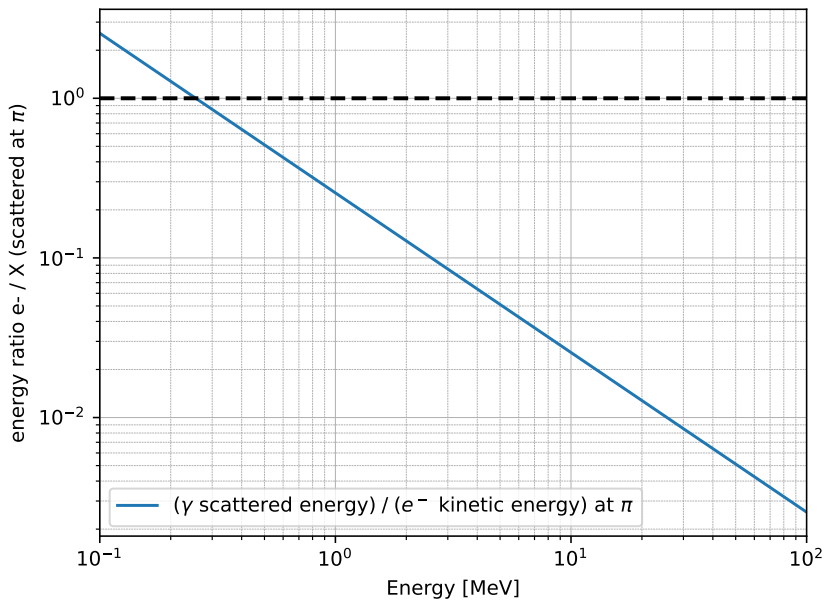

Calculation of dose from point kernels

(Ahnesjö and Aspradakis 1999)

Two-step procedure:

1. Ray-tracing primary photon trajectories (including beam modulators...) in a Cartesian matrix (cf Siddon 1985)
   $\Rightarrow$ Energy released in the patient
2. Dose is calculated by superposition of appropriately weighted kernels.

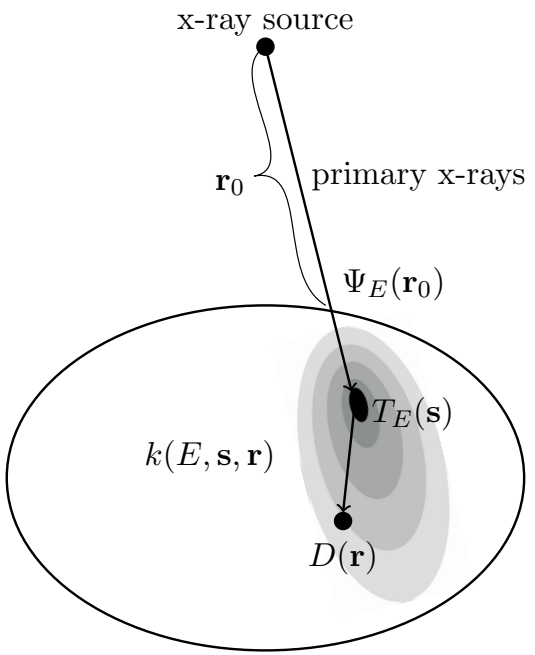

Scatter Dose

Complexity

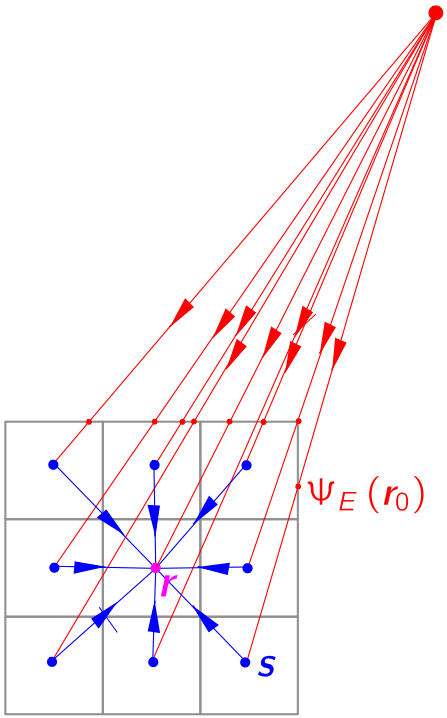

TERMA:

$$T_E(\mathbf{r}) = \Psi_E(\mathbf{r_0}) \left(\frac{r_0}{r}\right)^2 \exp\left(-\int_{\mathbf{r_0}}^{\mathbf{r}} \mu_E(\mathbf{l})\,\mathrm{d}l\right) \frac{\mu_E(\mathbf{r})}{\rho(\mathbf{r})}$$

Dose:

$$D(\mathbf{r}) = \frac{1}{\rho(\mathbf{r})} \iiint\!\!\iint T_E(\mathbf{s})\ \rho(\mathbf{s})\ h_E(\mathbf{r}-\mathbf{s})\ \mathrm{d}^3\mathbf{s}\,\mathrm{d}E$$

with kernel $h_E(\mathbf{r}-\mathbf{s})$ is the fraction of the radiant energy released by primary photons at $\mathbf{s}$ which is imparted per unit volume at $\mathbf{r}$

Complexity for a cubic volume of side N voxels:

- N^3 scattering points $\mathbf{s}$,
- N operations to raytrace between a scattering point and a receiving point
- computing dose $D(\mathbf{r})$ to N^3 receiving points $\mathbf{r}$

$\Rightarrow N^7$ number of operations for each energy E!

Polyenergetic case (1/4)

Brute force

Modification of the beam spectrum

- Hardening of the primary beam
  with angular dependency: stronger in the beam axis
- A single (mean) energy does not result in accurate dose values.

Brute-force solution: Simple sum

$$D_{\text{prim}}(\mathbf{r}) = \sum_E D_{\text{prim},E}(\mathbf{r})$$

$\Rightarrow$ Number of of bins: 5? 100? $\times$ longer than a single energy

Polyenergetic case (2/4)

(Ahnesjö 1989)

Weighted average over incident spectrum for each material m:

$$D(\mathbf{r}) = \frac{1}{\rho(\mathbf{r})} \iiint T_E(\mathbf{s})\ h_E(\mathbf{r}-\mathbf{s})\,\rho(\mathbf{s})\ \mathrm{d}^3\mathbf{s}\,\mathrm{d}E$$

becomes

$$D(\mathbf{r}) \approx \frac{1}{\rho(\mathbf{r})} \iiint \bar{T}(\mathbf{s})\ \bar{h}(\mathbf{r}-\mathbf{s})\,\rho(\mathbf{s})\ \mathrm{d}^3\mathbf{s}$$

with the "effective" TERMA

$$\bar{T}(\mathbf{r}) = \Psi(\mathbf{r_0}) \left(\frac{r_0}{r}\right)^2 \exp\left(-\int_{\mathbf{r_0}}^{\mathbf{r}} \bar{\mu}(\mathbf{l})\,\mathrm{d}l\right) \frac{\bar{\mu}(\mathbf{r})}{\rho(\mathbf{r})}$$

the "effective" attenuation coefficient

$$\bar{\mu}(\mathbf{r}) = \frac{\int \Psi_E(\mathbf{r_0})\ \mu_E(\mathbf{r})\ \mathrm{d}E}{\int \Psi_E(\mathbf{r_0})\ \mathrm{d}E}$$

and the "effective" kernel(s):

$$\bar{h}(\mathbf{r}) = \frac{\int \Psi_E(\mathbf{r_0})\ h_E(\mathbf{r})\ \mathrm{d}E}{\int \Psi_E(\mathbf{r_0})\ \mathrm{d}E}$$

Polyenergetic case (3/4)

(Ahnesjö and Aspradakis 1999)

Polyenergetic kernel averaged using TERMA-weighted contributions:

$$D(\mathbf{r}) = \frac{1}{\rho(\mathbf{r})} \iiint T_E(\mathbf{s})\ h_E(\mathbf{r}-\mathbf{s})\,\rho(\mathbf{s})\ \mathrm{d}^3\mathbf{s}\,\mathrm{d}E$$

with primary dose (e^-) vs scatter dose (γ) kernels

$$D(\mathbf{r}) \approx \frac{1}{\rho(\mathbf{r})} \iiint \left[\bar{T}_{\text{prim}}(\mathbf{s})\ \bar{h}_{\text{prim}}(\mathbf{r}-\mathbf{s}) + \bar{T}_{\text{scat}}(\mathbf{s})\ \bar{h}_{\text{scat}}(\mathbf{r}-\mathbf{s})\right] \mathrm{d}^3\mathbf{s}$$

- Compute weighted "effective" kernels

$$\bar{h}_{\text{prim}}(\mathbf{r}) = \frac{\int \Psi_E(\mathbf{r_0})\ h_{\text{p},E}(\mathbf{r})\,\mu_E(\mathbf{s})\,\mathrm{d}E}{\int \Psi_E(\mathbf{r_0})\,\mu_{\text{en},E}(\mathbf{s})\,\mathrm{d}E}$$

$$\bar{h}_{\text{scat}}(\mathbf{r}) = \frac{\int \Psi_E(\mathbf{r_0})\ h_{\text{p},E}(\mathbf{r})\,\mu_E(\mathbf{s})\,\mathrm{d}E}{\int \Psi_E(\mathbf{r_0})\,(\mu_E(\mathbf{s}) - \mu_{\text{en},E}(\mathbf{s}))\,\mathrm{d}E}$$

- Weighted integration over the spectrum of the primary and scatter kernels

$$\bar{T}_{\text{prim}}(\mathbf{s}) = \int T_E(\mathbf{s})\,\frac{\mu_{\text{en},E}(\mathbf{s})}{\mu_E(\mathbf{s})}\,\mathrm{d}E$$

$$\bar{T}_{\text{scat}}(\mathbf{s}) = \int T_E(\mathbf{s})\,\frac{\mu_E(\mathbf{s}) - \mu_{\text{en},E}(\mathbf{s})}{\mu_E(\mathbf{s})}\,\mathrm{d}E$$

Polyenergetic case (4/4)

(Ahnesjö, Veelen, and Tedgren 2017)

For the primary dose computation

$$K(\mathbf{r}) = \int \Psi_E(\mathbf{r_0}) \left(\frac{r_0}{r}\right)^2 \exp\left(-\int_{\mathbf{r_0}}^{\mathbf{r}} \mu_E(\mathbf{l})\,\mathrm{d}l\right) \frac{\mu_{\mathrm{en},E}(\mathbf{r})}{\rho(\mathbf{r})}\,\mathrm{d}E$$

Fit of the energy-dependent term at specific distances Δr for material m

$$\exp(-\bar{\mu}_m \Delta r)\ \bar{\mu}_{\mathrm{en},m} = \frac{\int \Psi_E(\mathbf{r_0})\ \exp(-\mu_{m,E}\Delta r)\ \mu_{\mathrm{en},m,E}\ \mathrm{d}E}{\int \Psi_E(\mathbf{r_0})\ \mathrm{d}E}$$

to get an expression of the KERMA not energy-dependent

$$K(\mathbf{r}) = \Psi(\mathbf{r_0}) \left(\frac{r_0}{r}\right)^2 \exp\left(-\int_{\mathbf{r_0}}^{\mathbf{r}} \bar{\mu}(\mathbf{l})\,\mathrm{d}l\right) \frac{\bar{\mu}_{\mathrm{en}}(\mathbf{r})}{\rho(\mathbf{r})}$$

Beam divergence

(Ahnesjö and Aspradakis 1999)

- Kernels should ideally be 'tilted'
- Tilt angle ν is calculated in the dose deposition point of view to avoid kernel rotation

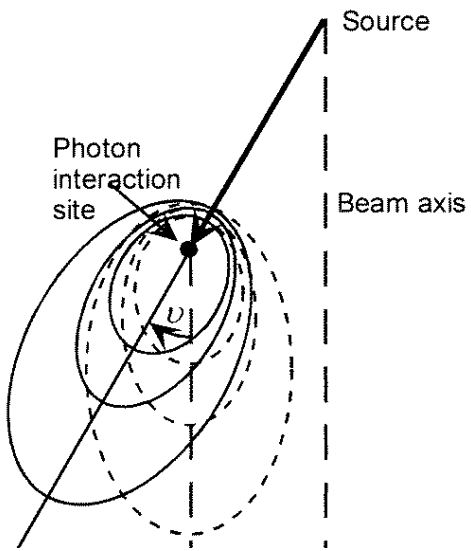

Explicit multiple-scatter dose kernel

Recursive calculations (Ahnesjö, Veelen, and Tedgren 2017)

A specific kernel for multiple-scatter dose from all higher order of scattering events can be introduced:

$$D = D_{\text{prim}} + (D_{1\text{sc}} + D_{\text{msc}})$$

Recall that the primary dose is defined by the primary collision KERMA

$$K(\mathbf{r}) = \frac{\bar{\mu}_{\text{en}}(\mathbf{r})}{\bar{\mu}(\mathbf{r})} T(\mathbf{r})$$

From $K(\mathbf{r})$ the first-scatter dose can be computed[1]

$$S_{1\text{sc}}(\mathbf{r}) = \frac{\bar{\mu}(\mathbf{r}) - \bar{\mu}_{\text{en}}(\mathbf{r})}{\bar{\mu}_{\text{en}}(\mathbf{r})} \frac{\bar{\mu}_{\text{en,1sc}}(\mathbf{r})}{\bar{\mu}_{1\text{sc}}(\mathbf{r})} K(\mathbf{r})$$

and from $S_{1\text{sc}}(\mathbf{r})$ the residual scatter dose can be computed

$$S_{\text{rsc}}(\mathbf{r}) = \frac{\bar{\mu}_{1\text{sc}}(\mathbf{r}) - \bar{\mu}_{\text{en,1sc}}(\mathbf{r})}{\bar{\mu}_{\text{en,1sc}}(\mathbf{r})} S_{1\text{st}}(\mathbf{r})$$

[1] S stands for SCERMA (SCattered Energy Released per unit MAss)

Plan

Collapsed Cone Convolution

Motivations behind the technique

3D Convolution issues:

- Kernel: singular at the origin, ie $h(r, \theta, \phi) = O\left(1/r^2\right)$ when $r \to 0$.
- Complexity: N^7 for a grid of N^3 voxels

Collapsed-Cone Convolution approximation:

(i) Cone collapsing in a discrete spherical coordinate system (r, θ, ϕ)
$\Rightarrow$ no more kernel singularity at $r = 0$

(ii) Set of 1D convolutions via recursive relations along transport lines

(iii) Lattice of transport lines (M over 4π)
$\Rightarrow$ Complexity $M\,N^3$

First introduced by Ahnesjö 1989, CCC is widely used in TPS such as Pinnacle (Philips), RayStation (RaySearch Laboratories), Monaco (Elekta CMS), Oncentra (Nucletron), and Mobius3D (Mobius Medical Systems).

Collapsed Cone Convolution

Concept (i): Collapsing

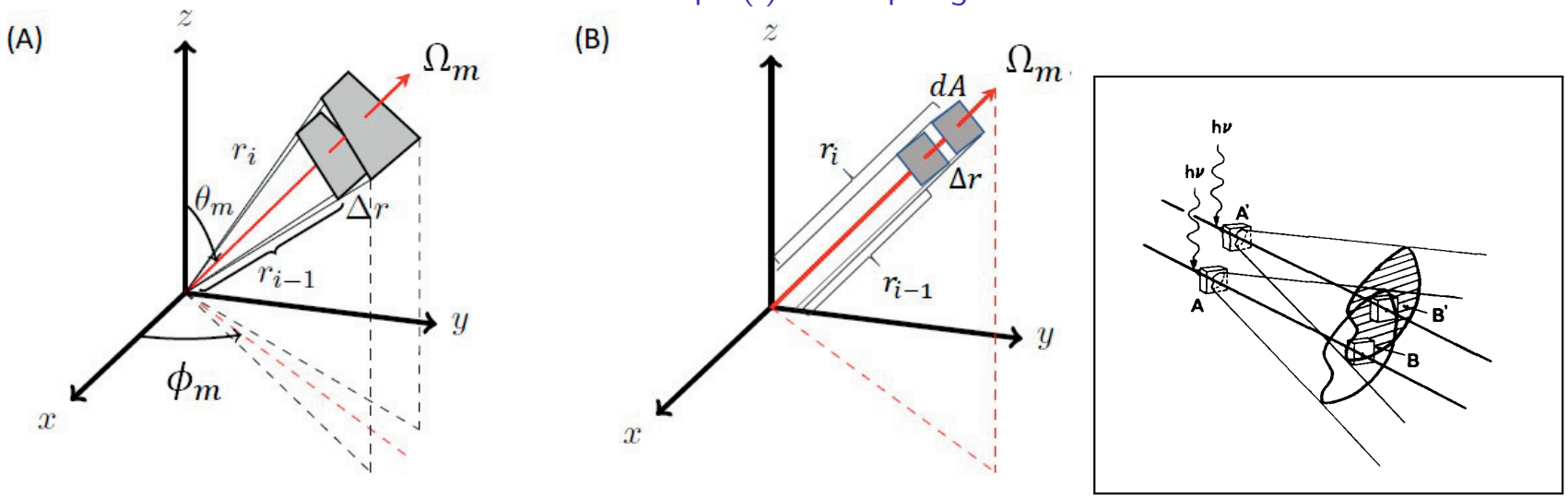

(A) Solid angle Ω_m subtended by cone element is collapsed to (B) infinitesimal area dA on the cone axis (from Battista 2019 and Ahnesjö 1989)

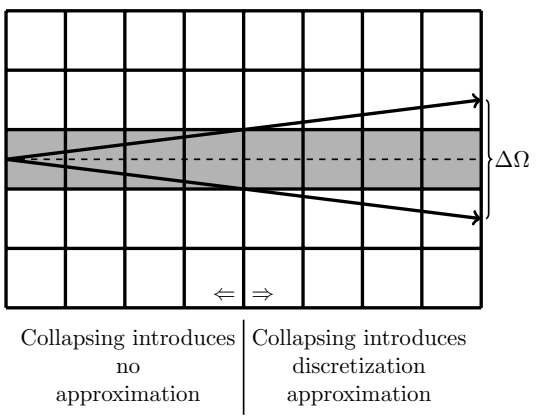

Collapsed Cone Convolution

Concept (ii): Recursivity

From the expression of the total energy fluence, the primary energy released in solid angle Ω_m

$$\mathcal{R}_m(r) = T(s)\,\rho(s)\,\mathrm{d}V \iint_{\Omega_m} \frac{1}{r^2}\left(\frac{A_\theta}{a_\theta} e^{-a_\theta L(r,\theta,\phi)} + \frac{B_\theta}{b_\theta} e^{-b_\theta L(r,\theta,\phi)}\right) \mathrm{d}\Omega$$

If we integrate over the solid angle Ω_m along direction $m \in M$

$$\mathcal{R}_m(r) = T(s)\,\rho(s)\,\mathrm{d}V\,\Omega_m \left(\frac{A_m}{a_m} e^{-a_m L(r,\theta,\phi)} + \frac{B_m}{b_m} e^{-b_m L(r,\theta,\phi)}\right)$$

with

$$L(r_i,\theta,\phi) = \sum_0^{r_i} \eta_i \Delta r_i$$

and the incremental (primary) radiant energy integrated from r_{i-1} to r_i

$$\Delta\mathcal{R}_{m,\mathrm{prim}}(r_i) = T_i\,\rho_i\,\mathrm{d}A\,\Omega_m \frac{A_m}{\eta_i a_m^2}\left(1 - e^{-a_m \eta_i \Delta r_i}\right)$$

and idem for the scatter radiant energy $\Delta\mathcal{R}_{m,\mathrm{scat}}(r_i)$

Collapsed Cone Convolution

Concept (iii): Transport lines

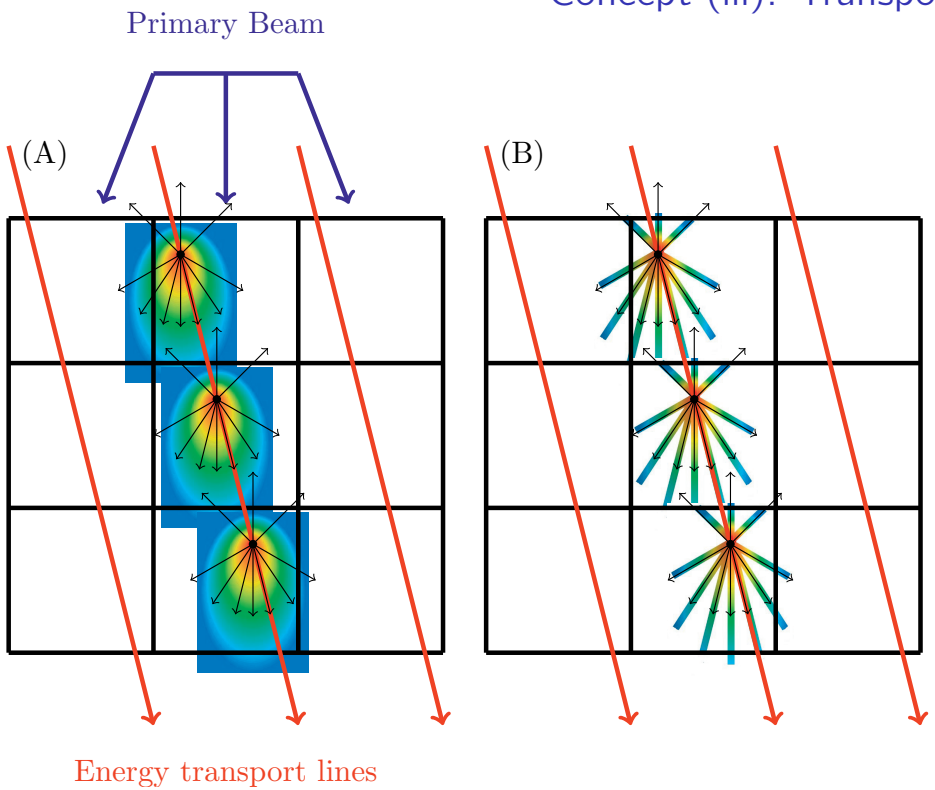

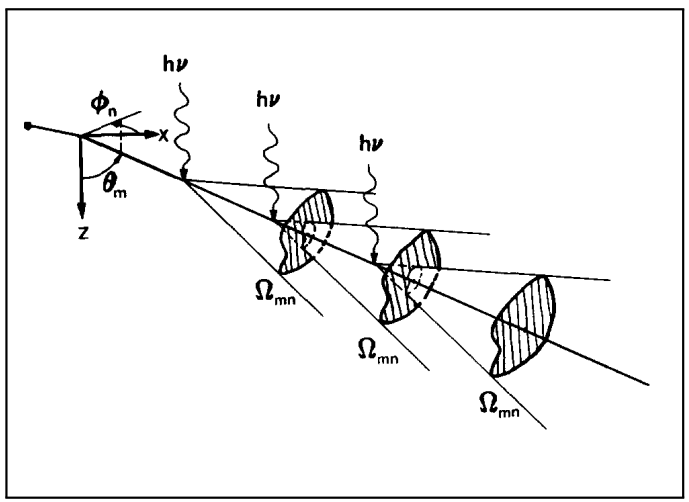

(A) Point kernels sampled with 10 cones ⇒ (B) radiant energy is released, transported, and attenuated along the transport lines.

(from Battista 2019 and Ahnesjö 1989)

⇒ for a given direction m, the radiant energy at a given voxel only depends on the **upstream cones**

Collapsed-Cone Convolution

Concept (iii): Transport lines

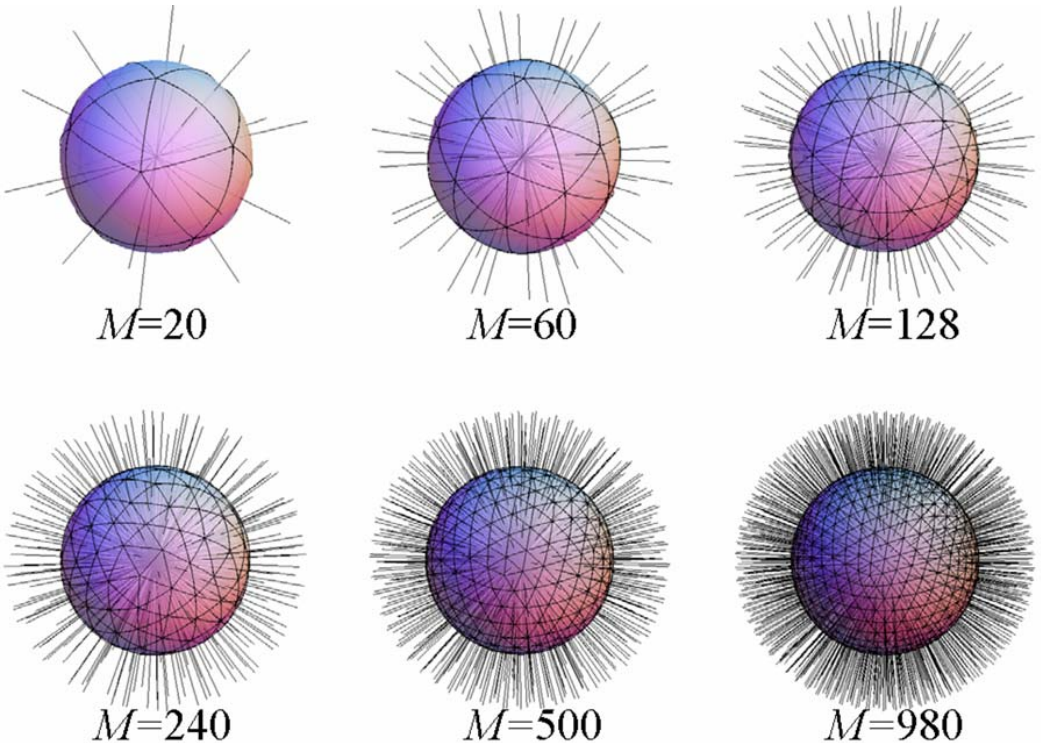

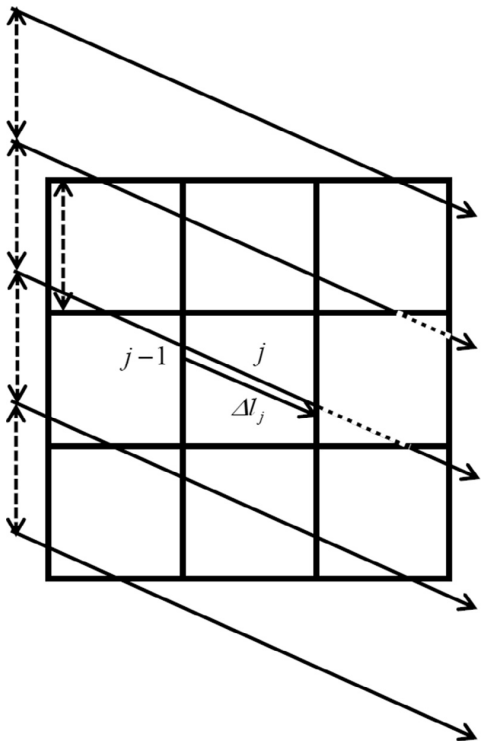

For each direction (θ_m, ϕ_n), a set of // is cast to cross all voxels.
The **passage for one voxel** is made **only once**.

(from Tedgren and Ahnesjö 2008 and Ahnesjö, Veelen, and Tedgren 2017)

Collapsed-Cone Convolution

Concept (iii): Transport lines

Algorithm:

- Select a direction m
  $\Rightarrow$ set of // lines across the volume
- For each line of the direction m: raytracing (Siddon 1985)
  1. start outside the irradiation field
  2. initialize the radiant energy to 0
  3. attenuate the radiant energy coming from the upstream cones
  4. add the radiant energy from the local cone

$$\mathcal{R}_{m,\text{prim}}(r_i) = \mathcal{R}_{m,\text{prim}}(r_{i-1})\ e^{-a_m \eta_i \Delta r_i} + \Delta\mathcal{R}_{m,\text{prim}}(r_i)$$

$$\mathcal{R}_{m,\text{scat}}(r_i) = \mathcal{R}_{m,\text{prim}}(r_{i-1})\ e^{-b_m \eta_i \Delta r_i} + \Delta\mathcal{R}_{m,\text{scat}}(r_i)$$

  5. go to step 3 for the next pixel along the line

Collapsed-Cone Convolution

Summary

Pre-processing:

- Beamline modeling for Monte Carlo simulations and precalculate kernels
- Analytical fitting of dose kernel parameters
- Dose measurements for calibration

Dose calculations:

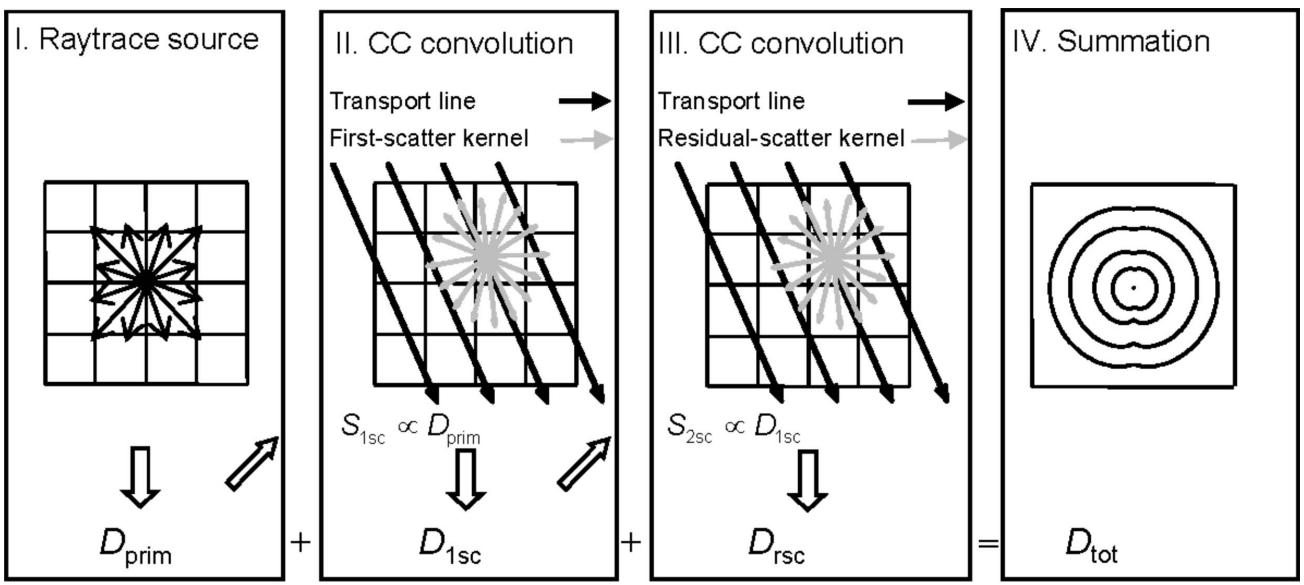

(from Tedgren and Ahnesjö 2008)

Plan

Pencil Beam Convolution

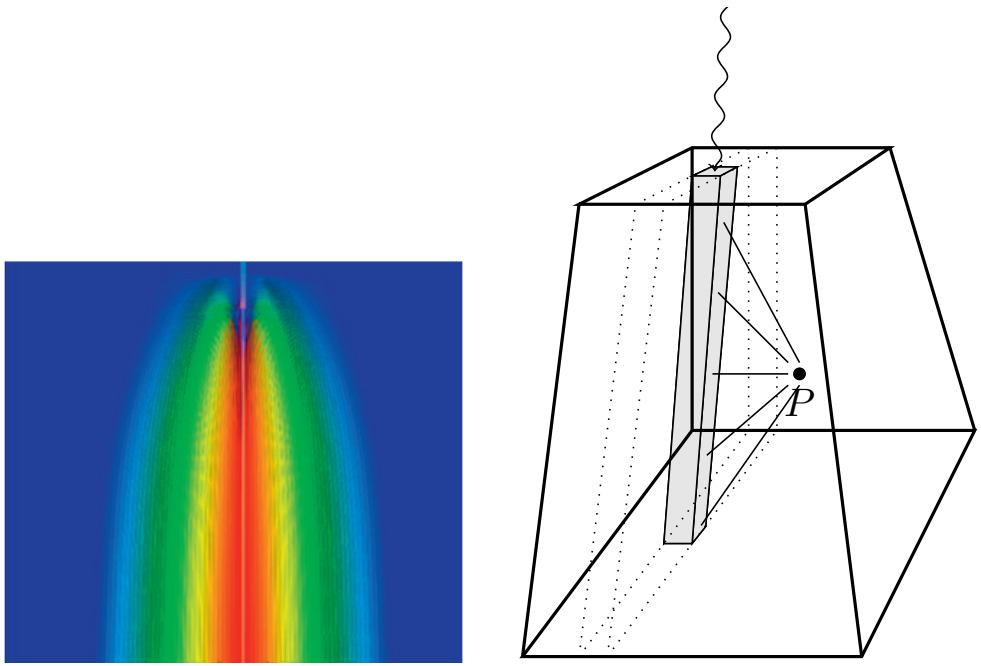

(from Battista 2019)

Motivation: Complexity N^5 when 3D convolution is N^7

Anisotropic Analytical Algorithm (AAA) introduced by Sievinen, Ulmer, and Kaissl 2005 and refined by Tillikainen et al. 2008, and implemented in the Eclipse TPS (Varian Medical Systems).

Analytical Anisotropic Algorithm

Dose spread kernel

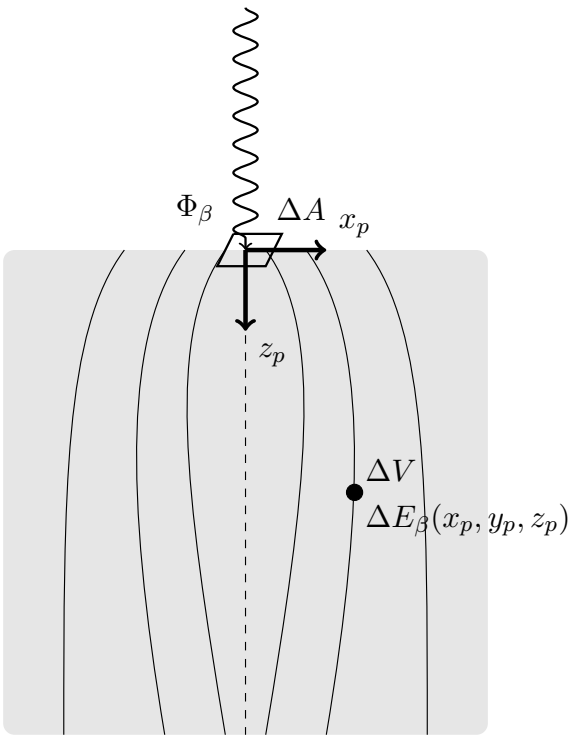

The dose (deposited energy per unit volume)

$$\frac{\Delta E_\beta\left(x_p, y_p, z_p\right)}{\Delta V} = \Phi_\beta \; \Delta A \; k_{z_p}\left(x_p, y_p\right)$$

where

- Φ_β s the fluence of the pencil beam with the area ΔA on the surface of the medium.
- $k_{z_p}\left(x_p, y_p\right)$ is the pencil-beam kernel (computed by MC simulations)

Analytical Anisotropic Algorithm

AAA

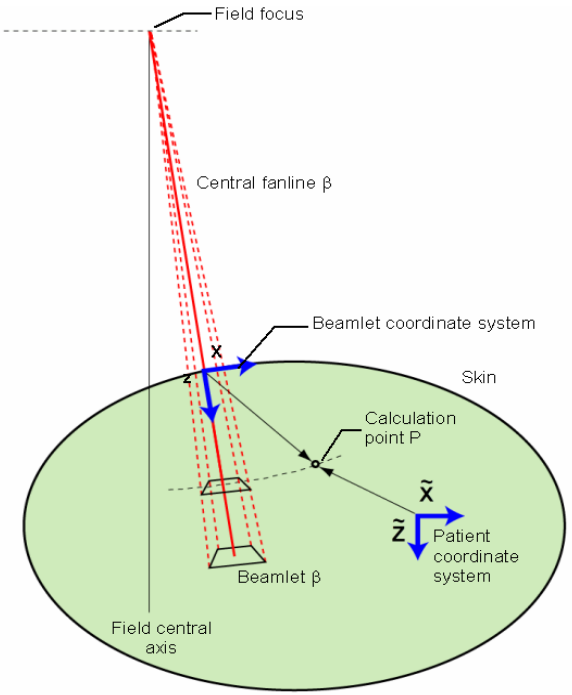

Two coordinate systems are used in the AAA algorithm:

- a non-Cartesian beamlet coordinate system (x_p, y_p, z_p) attached to each pencil beam
- a Cartesian coordinate system (x, y, z) associated with the patient

Analytical Anisotropic Algorithm

Pencil Beam kernel

The Monte-Carlo calculated pencil-beam kernel is factored into a product of a depth-dependent energy deposition function and a lateral scattering kernel.

$$k_{z_p}(x_p, y_p) = I_\beta(z_p)\ K_{z_p}(x_p, y_p)$$

with the depth-dependent function

$$I_\beta(z_p) = \iint_{\text{curved surface at } z_p} k_{z_p}(x_p, y_p)\, \mathrm{d}A$$

and the lateral scaling kernel

$$\iint_{\text{curved surface at } z_p} K_{z_p}(x_p, y_p)\, \mathrm{d}A \triangleq 1$$

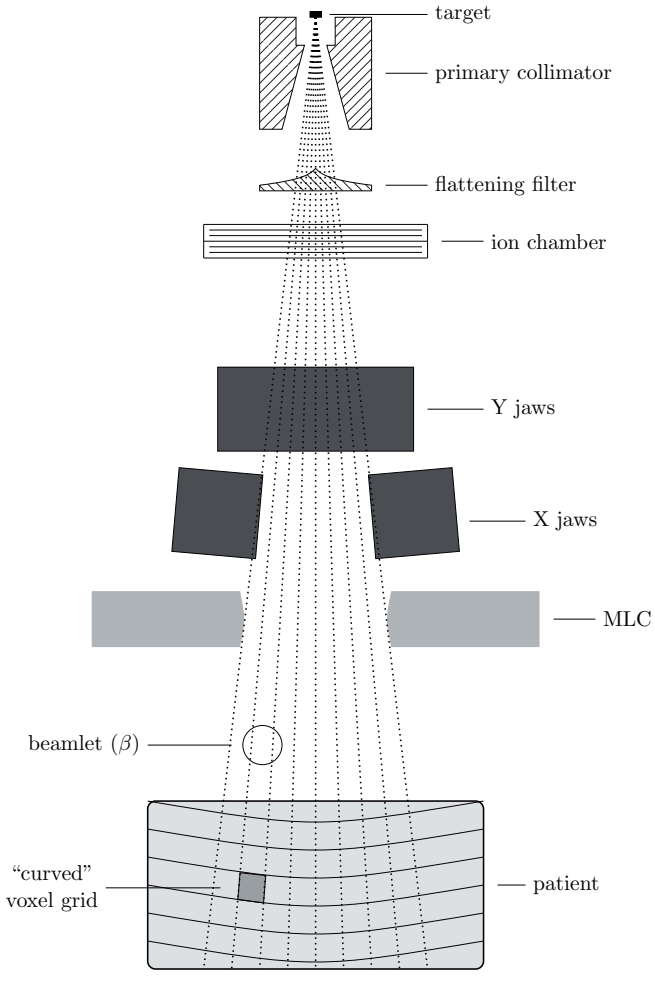

Analytical Anisotropic Algorithm

(Tillikainen et al. 2008)

The lateral scattering is modeled by an anisotropic analytical kernel (hence the algorithm name) with six exponential functions (originally 4 Gaussian),

$$K_{z_p}(x_p, y_p) = \frac{1}{r_p} \sum_{i=1}^{6} c_k(z_p)\ e^{-\mu_k r_p}$$

where μ_k are effective attenuation coefficients that are chosen by varying effective ranges $1/\mu_k$ from 1 to 200 mm with equal logarithmic intervals.

The approximation comes from the assumption that the density scaling can be performed along the depth and lateral directions independently.

Analytical Anisotropic Algorithm

Tissue Inhomogeneities

The depth-dependent function becomes ($\boldsymbol{\eta}(x_p, y_p, z_p)$ is the 3D volume of relative electron density)

$$I_\beta(z_p; \boldsymbol{\eta}) = \eta(0, 0, z_p)\, I_\beta(z_{\text{eff}})$$

with the effective depth

$$z_{\text{eff}} = \int_{z'_p=0}^{z_p} \eta\left(0, 0, z'_p\right) \mathrm{d}z'_p$$

and the lateral scaling kernel

$$K_{z_p}(x_p, y_p; \boldsymbol{\eta}) = \eta(x_p, y_p, z_p)\, \frac{1}{r_p} \sum_{i=1}^{6} c_k(z_{\text{eff}})\ e^{-\mu_k r_{\text{eff}}}$$

with the effective radius (SSD source-to-surface distance)

$$r_{\text{eff}} = \frac{SSD + z_{\text{eff}}}{SSD + z_p} \int_{r'_p=0}^{r_p} \eta\left(r'_p, z_p\right) \mathrm{d}r'_p$$

Analytical Anisotropic Algorithm

Summary

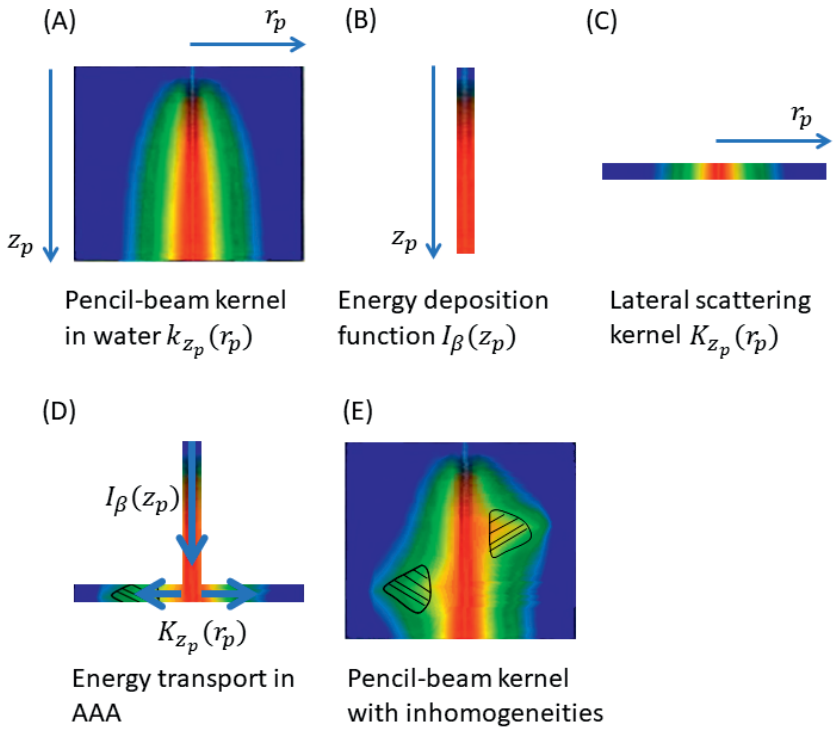

Total dose from primary photons (superposition of beamlet contributions)

$$D(x,y,z) = \frac{1}{\rho(x,y,z)} \sum_\beta \frac{\Delta E_\beta(x,y,z)}{\Delta V}$$

$\Rightarrow$ + extra-focal photons, electron contamination...

Plan

Boltzmann Transport Equation

Bedford 2019

Balance PDE equation

- for a given volume ΔV,
- for a given direction Ω,
- for a given particle type: γ, e^- or e^+.

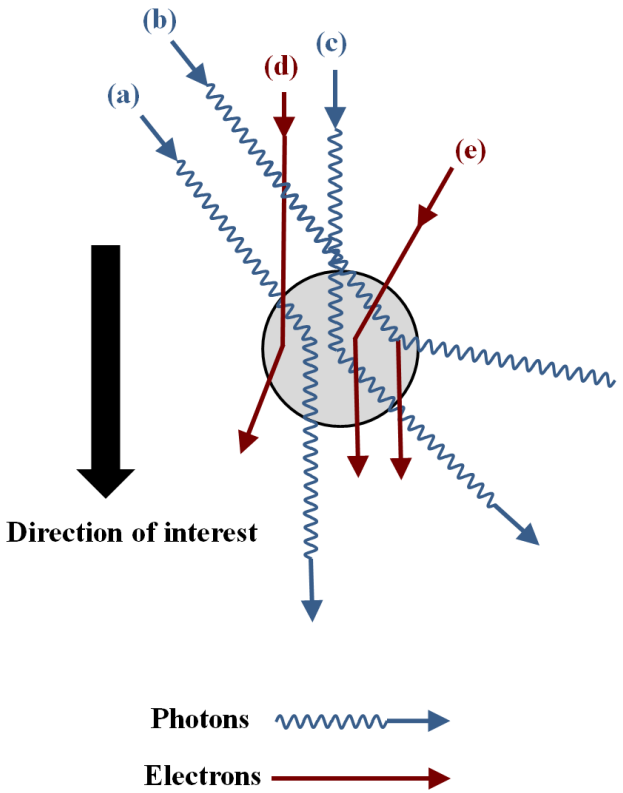

$$[\#\textbf{part OUT}] + [\#\textbf{part stopped}] = [\#\textbf{part IN}] + [\#\textbf{part produced}]$$

Boltzmann transport equation

Coupled Photon, Electron and Positron Formulation

Incoming Particles \ Outgoing Particles	$h\nu$	e^-	e^+
$h\nu$	Rayleigh Scatter Compton Scatter	Compton Scatter Pair Production Photoelectric	Pair Production
e^-	Bremsstrahlung	Elastic Scatter Möller Scatter	None
e^+	Bremsstrahlung Pair Annihilation	Bhabha Scatter	Elastic Scatter Bhabha Scatter

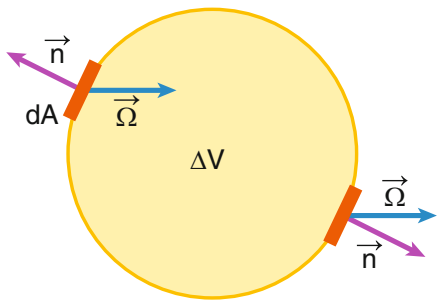

(from Battista 2019 and Vassiliev 2016)

Time independent set of equations:

$$\Omega \cdot \nabla \Phi^{\gamma} + \mu_t^{\gamma} \Phi^{\gamma} = q^{\gamma\gamma} + q^{e^-\gamma} + q^{e^+\gamma} + q^{\gamma}$$

$$\Omega \cdot \nabla \Phi^{e^-} + \mu_t^{e^-} \Phi^{e^-} = q^{e^-e^-} + q^{e^+e^-} + q^{\gamma e^-} + q^{e^-}$$

$$\Omega \cdot \nabla \Phi^{e^+} + \mu_t^{e^+} \Phi^{e^+} = q^{e^+e^+} + q^{\gamma e^+} + q^{e^+}$$

Boltzmann transport equation

Lewis 1984 & Vassiliev et al. 2010

Two classes of computational methods to solve the Boltzmann transport equation:

- deterministic with **grid-based Boltzmann solvers** (GBBS)
  $\Rightarrow$ discretization of the phase space
- stochastic numerical techniques with **Monte Carlo** (MC)
  $\Rightarrow$ random sampling of particles and processes

Both methods:

- achieve the **same level of accuracy**.
- are prone to errors:

Error type	GBBS	MC
stochastic		finite nr of particles
systematic	discretization approximations	condensed history VRT

Plan

Linear Boltzmann Transport Equation

Dose calculation

Historically, deterministic algorithms were developed primarily for solving problems of neutron transport (Lewis 1984)

Vassiliev et al. 2010 developed an implementation of the dose calculation in radiotherapy with photon beams:

- Explicit solution of the coupled 3D and time independent LBTE
- Discretization in space, angle and energy
- Iteratively solve the radiation transport

$\Rightarrow$ Acuros XB (AXB) algorithm implemented in the Eclipse TPS (Varian Medical Systems)

Grid-based Boltzmann Solvers

Standard approximations (Vassiliev et al. 2010)

The LTBE is difficult to solve in practice. Eg for photon transport:

$$\Omega \cdot \nabla \Phi^{\gamma} + \mu_t^{\gamma} \Phi^{\gamma} = q^{\gamma\gamma} + q^{e^-\gamma} + q^{e^+\gamma} + q^{\gamma}$$

and for the Compton contribution in the γ equation

$$q^{\gamma\gamma}(\mathbf{r}, \Omega, E) = \int_E \int_{4\pi} \sigma_{\text{Compton}}\left(E' \to E, \Omega \cdot \Omega'\right) \Phi^{\gamma}\left(\mathbf{r}, \Omega', E'\right) \, \mathrm{d}\Omega' \, \mathrm{d}E'$$

Additional basic assumptions can be made:

- $q^{e^-\gamma} = q^{e^+\gamma} = 0$, no radiative emission (local energy deposit)
- $q^{\gamma\gamma}$ events: Compton (and Rayleigh) scattering
  Restriction of photon fluences to just 2 components:
  - **unscattered**
  - **first scattered**

Grid-based Boltzmann Solvers

Standard approximations (Bedford 2019)

For electron transport

$$\Omega \cdot \nabla \Phi^{e^-} + \mu_t^{e^-} \Phi^{e^-} = q^{e^- e^-} + q^{\gamma e^-} + q^{e^+ e^-} + q^{e^-}$$

Several approximations have been proposed:

- No e^+, Pair Production
  $\Rightarrow$ two electrons instead of one electron and one positron
- $q^{e^- e^-}$ events: Møller scattering (inelastic) + Mott scattering (elastic)
  - Fokker–Planck approximation for highly peaked scattering
  - Continuous slowing down approximation (CSDA) for larger scattering

Grid-based Boltzmann Solvers

Phase space discretization (Lewis 1984)

To treat the **spatial** variable,

- Grid: Cartesian (voxelated model), tetrahedral, or triangulated mesh (see Reed and Hill 1973, Wareing et al. 2001)

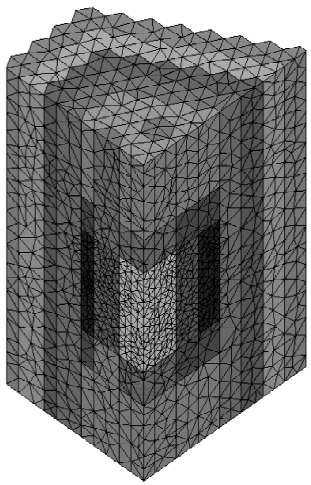

- Automatic built-in adaptation that increases element refinement near sharp beam gradients and heterogeneities.
- Model of fluence within each cell: constant, linear, with discontinuities at the boundaries.

Grid-based Boltzmann Solvers

Phase space discretization (Lewis 1984)

To treat **energy** variable,

- Multigroup method: cross-sections become piecewise constant
  $\Rightarrow$ integrals become sums.
- Generation of the appropriate group constants is not easy

To treat the **angular** variable,

- Moment expansions: Legendre polynomials or spherical harmonics
- Discrete ordinates method: solve the equations for discrete angles
- Hierarchical partition over 4π: adapt to the DCS
  (see Kópházi and Lathouwers 2015)

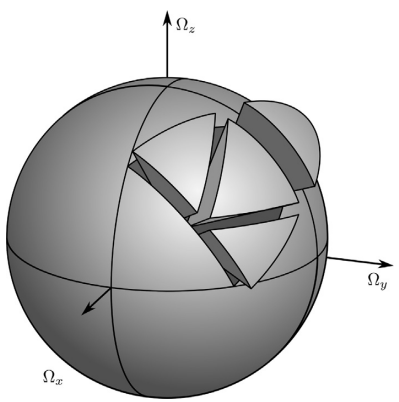

Grid-based Boltzmann Solvers

Iterative solution

Discretization of the phase space + Finite difference approximations $\Rightarrow$ linear matrix form

$$A\,\Phi = b$$

Iterative scheme: "source iteration"

- Series of sweeps for each of the angular quadrants
  $\Rightarrow$ From one voxel to the next in the direction of the radiation transport
- 1^{st} complete sweep = unscattered particles fluence,
- 2^{nd} sweep = 1^{st}-scattered particles,
- 3^{rd} sweep = 2^{nd}-scattered particles...

Grid-based Boltzmann Solvers

Absorbed Dose

Once the electron (and possibly positron) fluence is solved, the dose can be calculated from the **collisional stopping power** S_c:

$$D(\mathbf{r}) = \int_E \int_{4\pi} \frac{S_c}{\rho}(\mathbf{r}, E)\ \Phi^{e^-}(\mathbf{r}, \Omega, E)\ \mathrm{d}\Omega\, \mathrm{d}E$$

Plan

Dose deposition in analog MC

Energy deposition by e^-

- discrete when ionization/excitation
- continuous (condensed history)
  $\Rightarrow$ step limiter

But also by γ at interaction sites

- particle production cut
- modified process (eg no Fluorescence)
  $\Rightarrow$ local energy deposit

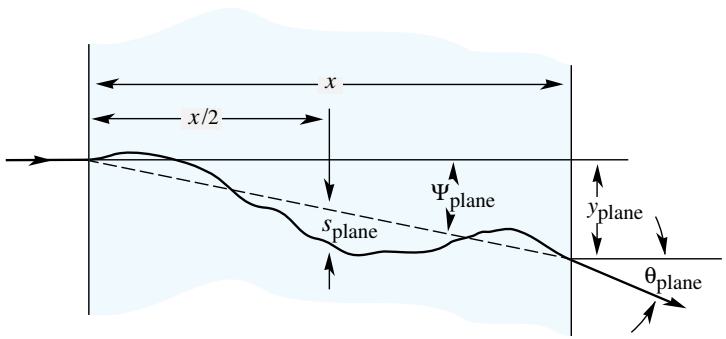

Multiple Coulomb scattering of charged particles, from Navas *et al.* (Particle Data Group) 2024

Variance Reduction Techniques

McGrath and Irving 1975; García-Pareja, Lallena, and Salvat 2021

- Sampling process (modified particle weights)
  - Russian Roulette / Splitting
  - Exponential Transform
  - Importance Sampling
  - Interaction Forcing
- Analytical equivalence
  - Expected values (TLE) $\rightarrow$ kV imaging dose
  - Correlated Sampling (same seed between runs)
- Specialized techniques
  - Sequential sampling (1^{st} low stat analog run then VRT)
  - Conditional MC
- Source modeling (avoid full MC simulation)
  - Virtual Energy Fluence (Fippel et al. 2003),
    Virtual Photon Source (Sikora, Dohm, and Alber 2007)
  - Phase Space (Jan et al. 2011)
  - Alpha-emitters (Sarrut, Etxebeste, and Létang 2024)

Implementations

- Standard Analog MC
  - GEANT4 (Allison et al. 2016)
  - PENELOPE (Salvat 2015)
  - EGSnrc (Kawrakow et al. 2013)
  - MCNPX (Waters et al. 2007)
- Ad-hoc Developments
  - GATE (Sarrut, Arbor, et al. 2022)
  - GAMOS (Arce et al. 2008)
  - TOPAS (Faddegon et al. 2020)
  - SimSET, PeneloPET...
- Optimized MC codes
  - Photon Voxel Monte Carlo algorithm XVMC (Fippel 1999) + GPU adaptation GPUMCD (Hissoiny et al. 2011)
  - Dose Planning Method DPM (Rodriguez et al. 2018)
  - BrachyDose, egs_brachy, ALGEBRA, RapidBrachyMCTPS, MCPI, HDRMC... (see review from Enger, Vijande, and Rivard 2020)

Plan

Ion RT, BNCT

- Same kinds of algorithms extended to proton or carbon ions):
  $\Rightarrow$ see the review of Saini et al. 2018 and De Martino et al. 2021
- Cell survival fraction: **Linear-Quadratic Model**

$$S = \exp\left(-\alpha D - \beta D^2\right)$$

  where α and β are exposure- and cell- specific parameters representing the number of lethal events
  $\Rightarrow$ α and β must be computed in **mixed fields** (weighted sums of the probability distribution of specific energy deposition)
- The **Relative Biological Effectiveness** (RBE):
  - Depends on the ion-specific linear energy transfer (LET)
  - Depends on the cell type (usually HSG is used)
- Various RBE models:
  - MKM: Microdosimetric Kinetic Model (Sato and Furusawa 2012)
  - LEM: Local Effect Model (Elsässer et al. 2010)
  - NanOx: Nanodosimetry and Oxidative stress model (Monini et al. 2020)

Final remarks

- Accuracy is no longer an issue with Monte Carlo or LBTE methods, but computation speed is (if used in the TPS optimization)
- Feasibility of MRI-only dose computation
- Time-resolved imaging issues
  - Organ (heart, lungs) motion: 4DCT...
  - Temporal biokinetics of injected radionuclides: SPECT...
- Use AI for dose calculations (very active field of research)
  $\Rightarrow$ quantification of the AI uncertainty (precision/bias)

Thank you for your attention

Ahnesjö, A (July 1989). "Collapsed cone convolution of radiant energy for photon dose calculation in heterogeneous media". In: Medical Physics 16.4, pp. 577–592. ISSN: 2473-4209. DOI: 10.1118/1.596360.

Ahnesjö, A and M M Aspradakis (1999). "Dose calculations for external photon beams in radiotherapy". In: Phys Med Biol 44, R99–R155.

Ahnesjö, A, B van Veelen, and Å C Tedgren (Feb. 2017). "Collapsed cone dose calculations for heterogeneous tissues in brachytherapy using primary and scatter separation source data". In: Computer Methods and Programs in Biomedicine 139, pp. 17–29. ISSN: 0169-2607. DOI: 10.1016/j.cmpb.2016.10.022.

Allison, J et al. (Nov. 2016). "Recent developments in Geant4". In: Nuclear Instruments and Methods in Physics Research Section A: Accelerators, Sp 835, pp. 186–225. DOI: 10.1016/j.nima.2016.06.125.

Arce, P et al. (Oct. 2008). "GAMOS: A Geant4-based easy and flexible framework for nuclear medicine applications". In: 2008 IEEE Nuclear Science Symposium Conference Record. IEEE. DOI: 10.1109/nssmic.2008.4775023.


Battista, J, ed. (2019). Introduction to megavoltage x-ray dose computation algorithms. Series in Medical Physics and Biomedical Engineering. Boca Raton, FL: CRC Press. 1418 pp. ISBN: 135167613X.


Bedford, J L (Jan. 2019). "Calculation of absorbed dose in radiotherapy by solution of the linear Boltzmann transport equations". In: Physics in Medicine & Biology 64.2, 02TR01. ISSN: 1361-6560. DOI: 10.1088/1361-6560/aaf0e2.


De Martino, F et al. (July 2021). "Dose Calculation Algorithms for External Radiation Therapy: An Overview for Practitioners". In: Applied Sciences 11.15, p. 6806. ISSN: 2076-3417. DOI: 10.3390/app11156806.


Elsässer, T et al. (Nov. 2010). "Quantification of the Relative Biological Effectiveness for Ion Beam Radiotherapy: Direct Experimental Comparison of Proton and Carbon Ion Beams and a Novel Approach for Treatment Planning". In: International Journal of Radiation Oncology*Biology*Physics 78.4, pp. 1177–1183. ISSN: 0360-3016. DOI: 10.1016/j.ijrobp.2010.05.014.

 Enger, S A, J Vijande, and M J Rivard (Jan. 2020). "Model-Based Dose Calculation Algorithms for Brachytherapy Dosimetry". In: Seminars in Radiation Oncology 30.1, pp. 77–86. ISSN: 1053-4296. DOI: 10.1016/j.semradonc.2019.08.006.

 Faddegon, B et al. (Apr. 2020). "The TOPAS tool for particle simulation, a Monte Carlo simulation tool for physics, biology and clinical research". In: Physica Medica 72, pp. 114–121. ISSN: 1120-1797. DOI: 10.1016/j.ejmp.2020.03.019.

 Fippel, M (Aug. 1999). "Fast Monte Carlo dose calculation for photon beams based on the VMC electron algorithm". In: Medical Physics 26.8, pp. 1466–1475. ISSN: 0094-2405. DOI: 10.1118/1.598676.

 Fippel, M et al. (Feb. 2003). "A virtual photon energy fluence model for Monte Carlo dose calculation". In: Medical Physics 30.3, pp. 301–311. ISSN: 2473-4209. DOI: 10.1118/1.1543152.

 García-Pareja, S, A M Lallena, and F Salvat (Oct. 2021). "Variance-Reduction Methods for Monte Carlo Simulation of Radiation Transport". In: 9. DOI: 10.3389/fphy.2021.718873.

González, W et al. (Dec. 2015). "A general photon source model for clinical linac heads in photon mode". In: Radiation Physics and Chemistry 117, pp. 140–152. ISSN: 0969-806X. DOI: 10.1016/j.radphyschem.2015.08.006.

Hissoiny, S et al. (Jan. 2011). "GPUMCD: A new GPU-oriented Monte Carlo dose calculation platform". In: Medical Physics 38.2, pp. 754–764. ISSN: 2473-4209. DOI: 10.1118/1.3539725.

Jan, S et al. (2011). "GATE V6: a major enhancement of the GATE simulation platform enabling modelling of CT and radiotherapy". In: Physics in medicine and biology 56.4, p. 881. DOI: 10.1088/0031-9155/56/4/001.

Kawrakow, I et al. (2013). EGSnrc: software for Monte Carlo simulation of ionizing radiation. en. NRCC Report PIRS-701. DOI: 10.4224/40001303.

Kópházi, J and D Lathouwers (Sept. 2015). "A space-angle DGFEM approach for the Boltzmann radiation transport equation with local angular refinement". In: Journal of Computational Physics 297, pp. 637–668. ISSN: 0021-9991. DOI: 10.1016/j.jcp.2015.05.031.

Lewis, E E (1984). Computational methods of neutron transport. Wiley, p. 401. ISBN: 0471092452.

 McGrath, E J and D C Irving (Apr. 1975). Techniques for efficient Monte Carlo simulation. Vol. III. Variance reduction. Science Applications. URL: https://www.osti.gov/biblio/4210677.

 Monini, C et al. (Feb. 2020). "Determination of the Effective Local Lethal Function for the NanOx Model". In: Radiation Research 193.4, p. 331. DOI: 10.1667/rr15463.1.

 Navas *et al.* (Particle Data Group), S (2024). "Review of particle physics". In: Phys. Rev. D 110.030001. DOI: 10.1103/PhysRevD.110.030001.

 Reed, W H and T R Hill (1973). Triangular mesh methods for the neutron transport equation. Tech. rep. Los Alamos Scientific Lab., N. Mex.(USA).

 Rodriguez, M et al. (Dec. 2018). "DPM as a radiation transport engine for PRIMO". In: Radiation Oncology 13.1. ISSN: 1748-717X. DOI: 10.1186/s13014-018-1188-6.

- Saini, J et al. (Apr. 2018). "Advanced Proton Beam Dosimetry Part I: review and performance evaluation of dose calculation algorithms". In: Translational Lung Cancer Research 7.2, pp. 171–179. ISSN: 2226-4477. DOI: 10.21037/tlcr.2018.04.05.
- Salvat, F (2015). "PENELOPE-2014: A Code System for Monte Carlo Simulation of Electron and Photon Transport". In: OECD-NEA Data Bank.
- Sarrut, D, N Arbor, et al. (Aug. 2022). "The OpenGATE ecosystem for Monte Carlo simulation in medical physics". In: Physics in Medicine & Biology 67.18, p. 184001. DOI: 10.1088/1361-6560/ac8c83.
- Sarrut, D, A Etxebeste, and J M Létang (Apr. 2024). "A photon source model for alpha-emitter radionuclides". In: Physics in Medicine & Biology 69.9, p. 095009. ISSN: 1361-6560. DOI: 10.1088/1361-6560/ad3881.
- Sato, T and Y Furusawa (Oct. 2012). "Cell Survival Fraction Estimation Based on the Probability Densities of Domain and Cell Nucleus Specific Energies Using Improved Microdosimetric Kinetic Models". In: Radiation Research 178.4, pp. 341–356. ISSN: 1938-5404. DOI: 10.1667/rr2842.1.

Siddon, R L (Mar. 1985). "Fast calculation of the exact radiological path for a three-dimensional CT array". In: Medical Physics 12.2, pp. 252–255. ISSN: 2473-4209. DOI: 10.1118/1.595715.

Sievinen, J, W Ulmer, and W Kaissl (2005). AAA Photon Dose Calculation Model in Eclipse^{TM}. Tech. rep. 2894. Varian Medical Systems.

Sikora, M, O Dohm, and M Alber (June 2007). "A virtual photon source model of an Elekta linear accelerator with integrated mini MLC for Monte Carlo based IMRT dose calculation". In: Physics in Medicine and Biology 52.15, pp. 4449–4463. ISSN: 1361-6560. DOI: 10.1088/0031-9155/52/15/006.

Tedgren, Å C and A Ahnesjö (2008). "Optimization of the computational efficiency of a 3D, collapsed cone dose calculation algorithm for brachytherapy". In: Medical Physics 35.4, pp. 1611–1618.

Tillikainen, L et al. (June 2008). "A 3D pencil-beam-based superposition algorithm for photon dose calculation in heterogeneous media". In: Physics in Medicine and Biology 53.14, pp. 3821–3839. ISSN: 1361-6560. DOI: 10.1088/0031-9155/53/14/008.


Vassiliev, O N (Oct. 26, 2016). Monte Carlo Methods for Radiation Transport. Springer International Publishing. 300 pp. ISBN: 331944140X. URL: https://www.ebook.de/de/product/26469127/oleg_n_vassiliev_monte_carlo_methods_for_radiation_transport.html.


Vassiliev, O N et al. (Jan. 2010). "Validation of a new grid-based Boltzmann equation solver for dose calculation in radiotherapy with photon beams". In: Physics in Medicine and Biology 55.3, pp. 581–598. ISSN: 1361-6560. DOI: 10.1088/0031-9155/55/3/002.


Wareing, T A et al. (July 2001). "Discontinuous Finite Element S_N Methods on Three-Dimensional Unstructured Grids". In: Nuclear Science and Engineering 138.3, pp. 256–268. ISSN: 1943-748X. DOI: 10.13182/nse138-256.


Waters, L S et al. (2007). "The MCNPX Monte Carlo radiation transport code". In: Hadronic Shower Simulation Workshop (AIP Conference Proceedings Volume 896 Vol. 896, pp. 81–90.